Check for updates

AGU ADVANCING EARTH AND SPACE SCIENCES

AGU Advances

RESEARCH ARTICLE
10.1029/2026AV002570

Brine Pool Microbes Enrich Metalliferous Sediments in Salt Giant Basins

Morgan I. Chakraborty[1], Hannah Shernisky[1], Clément G. L. Pollier[1], Amanda M. Oehlert[1], Arash Sharifi[1,2], Ali Pourmand[1], Bolton J. Howes[1], Benjamin Minch[3], Mohammad Moniruzzaman[3], Larissa Frühe[4], Mattie Rodrigue[4], and Sam J. Purkis[1]

[1]Department of Marine Geosciences, Rosenstiel School of Marine, Atmospheric, and Earth Science, University of Miami, Miami, FL, USA, [2]SGS-Isobar Science, Miami, FL, USA, [3]Department of Marine Biology and Ecology, Rosenstiel School of Marine, Atmospheric, and Earth Science, University of Miami, Miami, FL, USA, [4]OceanX, New York, NY, USA

Peer Review The peer review history for this article is available as a PDF in the Supporting Information.

Key Points:

- Red Sea brine pools are ephemeral
- Microbes within these brine pools enrich metals and trace elements 10× to 117×, and the enrichment persists into the geological record
- Such deposits aid understanding of early life on Earth and the search for life beyond it

Supporting Information:

Supporting Information may be found in the online version of this article.

Correspondence to:

M. I. Chakraborty,
morgan.chakraborty@earth.miami.edu

Citation:

Chakraborty, M. I., Shernisky, H., Pollier, C. G. L., Oehlert, A. M., Sharifi, A., Pourmand, A., et al. (2026). Brine pool microbes enrich metalliferous sediments in salt giant basins. *AGU Advances*, *7*, e2026AV002570. https://doi.org/10.1029/2026AV002570

Received 8 MAY 2026
Accepted 17 AUG 2026

Author Contributions:

Conceptualization: Morgan I. Chakraborty, Sam J. Purkis
Data curation: Morgan I. Chakraborty, Bolton J. Howes, Benjamin Minch, Mohammad Moniruzzaman, Sam J. Purkis
Formal analysis: Morgan I. Chakraborty, Hannah Shernisky, Clément G. L. Pollier, Amanda M. Oehlert, Arash Sharifi, Ali Pourmand, Benjamin Minch, Mohammad Moniruzzaman, Sam J. Purkis
Funding acquisition: Sam J. Purkis
Investigation: Morgan I. Chakraborty, Clément G. L. Pollier, Amanda M. Oehlert, Arash Sharifi, Ali Pourmand, Sam J. Purkis

© 2026 The Author(s). AGU Advances published by Wiley Periodicals LLC on behalf of American Geophysical Union. This is an open access article under the terms of the Creative Commons Attribution License, which permits use, distribution and reproduction in any medium, provided the original work is properly cited.

Abstract We report the discovery of an extinct deep-sea brine pool in the Red Sea's Hume Deep, providing evidence that rift-shoulder pools are ephemeral on millennial timescales, and that the microbially-enriched metalliferous deposits produced during the pool's active phase persist into the stratigraphic record. Now devoid of brine, the Hume Deep retains signatures of activity, including a well-preserved Lagerstätte death assemblage, seafloor staining consistent with past inhabitation by extremophile microbes, and enrichment of metals associated with their metabolisms. Elemental analyses of seafloor sediments demonstrate that the high metal concentrations in the Hume Deep match those of the active NEOM brine pool, situated 90 km north. In the NEOM pool, metagenomics and metatranscriptomics, coupled with scanning electron microscopy and energy-dispersive spectroscopy, suggest that microbes drive metal enrichment via microbe-mineral interactions up to 117× higher than background values. These results suggest a role for microbial processes in metalliferous sediment formation in deep-sea brine pools. Uranium-thorium dating suggests the Hume pool was last active between two and 16 thousand years ago. We propose that rift-shoulder brine pools fill and drain in response to tectonically controlled hydrothermal circulation. Our findings suggest that: (a) microbes inhabiting ancient Red Sea brine pools radically enhanced the metalliferous content of the stratigraphy within and above the basin's Miocene evaporites, and (b) that the elemental composition of other salt giant basins might have been similarly microbially mediated. With implications for understanding early life on Earth, our results provide a framework for interpreting deep-sea metal enrichments in modern and ancient extremophile environments.

Plain Language Summary Metals like iron, potassium, manganese, copper, and molybdenum are known to accumulate in deep-sea brine pools, usually through interactions between sediments, seawater, and hydrothermal fluids. Our new research in the deep Red Sea reveals a surprising biological mechanism behind this metal enrichment. We found that microbes living in the oxygen-free brine help concentrate these elements in sediments—sometimes to levels more than one hundred times higher than those on the normal seafloor. This discovery matters for two reasons. First, many of these metals are essential for clean energy technologies, and understanding how they accumulate could help guide future resource exploration. Second, these brine pools offer a rare glimpse into how early life on Earth may have functioned. We show that sharp rises in manganese levels in ancient oceans may not have been caused by oxygen alone, but could also have come from microbial activity. Our findings give scientists a new tool for identifying early life and interpreting the chemical clues left behind in ancient rocks.

1. Introduction

Metalliferous marine sediments have long been recognized as geochemically distinctive deposits, but have received renewed attention because of their potential relevance to critical raw materials and the global energy transition (Bostrom & Peterson, 1966). Such deposits are often found in association with deep-sea brine pools (Bäcker & Richter, 1973; Zierenberg, 1990) and can host valuable concentrations of transition elements—manganese, copper, iron, and molybdenum—plus other rare-earth elements (Boström & Peterson, 1969; Meylan et al., 2012). For brevity, we will refer to this portfolio of commercially-important elements (Mn, Cu, K, Fe, Mo) as "metals and trace elements." As a consequence of the alternative energy revolution, including initiatives like Net Zero 2050, metals and trace elements are receiving sharp attention; global demand is rapidly outstripping supply (Jones, 2023; Vysetti, 2023).

Methodology: Morgan I. Chakraborty, Hannah Shernisky, Larissa Frühe, Mattie Rodrigue, Sam J. Purkis
Project administration: Sam J. Purkis
Resources: Morgan I. Chakraborty, Sam J. Purkis
Software: Morgan I. Chakraborty, Sam J. Purkis
Supervision: Sam J. Purkis
Validation: Morgan I. Chakraborty, Sam J. Purkis
Visualization: Morgan I. Chakraborty, Amanda M. Oehlert, Bolton J. Howes, Sam J. Purkis
Writing – original draft: Morgan I. Chakraborty
Writing – review & editing: Morgan I. Chakraborty, Clément G. L. Pollier, Amanda M. Oehlert, Arash Sharifi, Ali Pourmand, Bolton J. Howes, Benjamin Minch, Mohammad Moniruzzaman, Larissa Frühe, Mattie Rodrigue, Sam J. Purkis

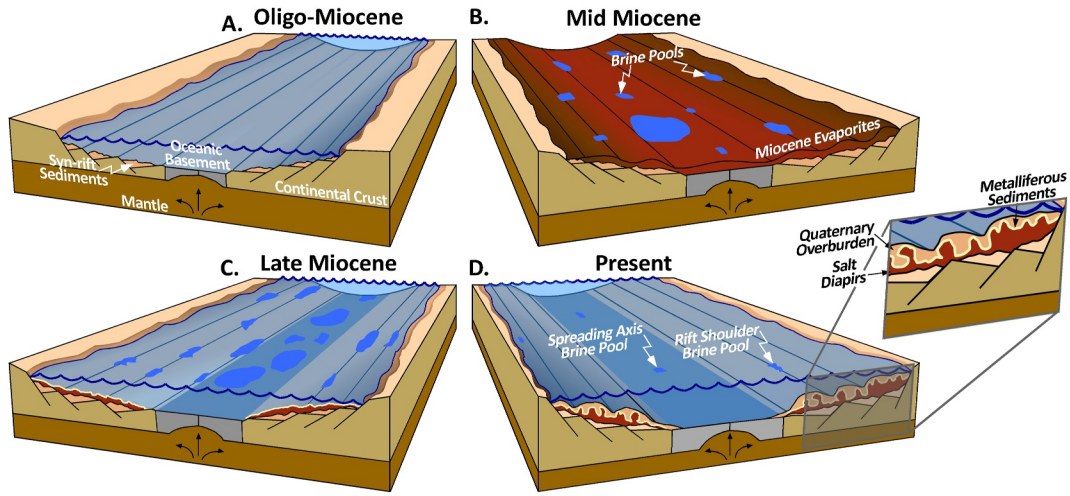


Figure 1. Conceptual model for brine pool evolution in an extensional basin. (a) The initial phase of basin opening allows seawater to enter, as occurred in the Oligo-Miocene for the Red Sea. (b) Progressive restriction from the open ocean promotes desiccation and widespread evaporite accumulation, corresponding to massive halite deposition during the Mid Miocene in the Red Sea. These freshly deposited evaporites are broadly exposed to seawater when the basin refloods, in the Late Miocene (c). Halite dissolution delivers a brief episode of abundant Red Sea brine pools, which are gradually extinguished by the deposition of the Quaternary hemipelagite overburden, leading to the modern situation, (d), where just a small number of pools occupy the basin, associated either with the rift spreading axis, else with faulting along the rift shoulders. Not to scale.

Anoxic brine pools are more common in the deep sea than once thought, but their discovery is limited by sparse exploration and their isolated, patchwork distribution. Notable examples occur in the Gulf of Mexico, the Mediterranean, and the Red Sea, and many are thought to have formed through the dissolution of subsurface evaporites deposited during past episodes of basin desiccation (Camerlenghi, 1990; Craig, 1966; Delaunay et al., 2023; Joye et al., 2005; Pensa, 2024; Pensa, Baby, et al., 2025; Pensa, Huertas, & Afifi, 2025; Purkis et al., 2025).

The elemental composition of deep-sea sediments associated with brine pools can be set by a variety of mechanisms, ranging from hydrothermal processes to microbial metabolisms. One mechanism driving enriched metal concentration in seafloor sediments is precipitation from hydrothermal fluids (Backer & Schoell, 1972; Corliss, 1971; Corliss et al., 1978; Cronan, 1979; Rona, 1978; Spooner & Fyfe, 1973; Weiss, 1977). The Thetis Deep, located on the Red Sea's central spreading axis, provides one such example of a hydrothermal brine system (Pierret et al., 2010). In contrast, microbial processes offer another means of enriching metals through three predominant pathways—biomineralization, bioaccumulation/biosorption, and biologically mediated redox reactions (Ams et al., 2013; Dupraz et al., 2009; Gadd, 2010; Harris, 2017; Krumbein, 1983; Wang et al., 2013). The prokaryotes involved in these metal-concentrating mechanisms thrive in anoxic hypersaline environments, once thought inhospitable to life, but previous studies reveal that anoxic deep-sea brine pools actually harbor oases of halophilic microbes (Antunes et al., 2011; Danovaro et al., 2010; Minch et al., 2024; Purkis et al., 2022; Rothschild & Mancinelli, 2001).

Extremophile microbes—prokaryotes living in extreme physical and/or chemical conditions—which inhabit deep-sea brine pools can enrich sediments with metals to concentrations orders of magnitude higher than in the surrounding oxygenated seabed (Wang et al., 2013). Despite such elevated concentrations, these metalliferous sediments may be volumetrically inconsequential because modern brine pools are rare and small. For example, by our calculation, the pools so far discovered in the Red Sea occupy less than 0.1% of the area of the 440,000 km^2 basin. But are modern conditions a good analog for the geological past? Perhaps not. We posit that brine pools were both large and abundant when, (a) their host "salt giant" basins initially formed, and then, (b) when those basins reflooded after desiccation events. We explore this theory through a conceptual model of the genesis of brine pools in the Red Sea rift (Figure 1) and contend that it broadly applies to brine pool formation in other salt basins throughout geological time.

2576604x, 2026, 6, Downloaded from https://agupubs.onlinelibrary.wiley.com/doi/10.1029/2026AV002570 by Readcube (Labtiva Inc.), Wiley Online Library on [14/10/2026]. See the Terms and Conditions (https://onlinelibrary.wiley.com/terms-and-conditions) on Wiley Online Library for rules of use; OA articles are governed by the applicable Creative Commons License

2. The Origin of Brine Pools in the Red Sea

Red Sea rifting initiated in the Oligocene. Via a connection to the Mediterranean, the proto-Red Sea was first flooded by normal marine waters about 24.5 mya (Segev et al., 2017) (Figure 1a). Then, in the Mid Miocene, the basin was isolated from the Mediterranean, initiating a salinity crisis, which deposited evaporite sequences that locally exceed 2.5 km in thickness (Heaton et al., 1995; Petrovic et al., 2023). Evaporite-rich sequences deposited during this crisis include the Mansiyah Salt, deposited 14.0–13.2 mya (Hughes et al., 1999; Tubbs et al., 2014), overlain by the Ghawwas Formation, a siliciclastic unit interbedded with anhydrite which was deposited 13.2–6.2 mya (Baby et al., 2024; Hughes & Johnson, 2005; Pensa, 2024). Given that the Gulf of Aqaba only formed 14–11 mya (Bosworth et al., 2018; Stockli & Bosworth, 2018), it is likely that evaporites in this pull-apart basin can predominantly be ascribed to the Ghawwas Formation and more recent evaporitic episodes, with only minor contribution from the older Mansiyah Salt.

The precise origin of the Red Sea and Gulf of Aqaba evaporites is still an open question. Solar evaporation of seawater likely contributed to their formation, but Pensa (2024) estimated that >50 evaporation cycles would be required to account for the thickness of salt observed in the Red Sea, which can locally exceed 2.5 km. So many cycles seem unlikely, and would need to be coupled to an exceedingly rapid rate of basin subsidence (Heaton et al., 1995). Whereas the radiogenic strontium (Sr) value of the salt supports evaporation of Miocene seawater (Chakraborty et al., 2025), several thin horizons in the Mansiyah and Ghawwas display conspicuously low radiogenic Sr isotope ratios, suggesting the influence of fluids which interacted with the mantle (Pensa, 2024; Pensa, Baby, et al., 2025; Pensa, Huertas, & Afifi, 2025). Low radiogenic Sr isotope ratios support two additional mechanisms of salt production: via hydrothermal processes (Hovland et al., 2015) and via mantle serpentinization (Debure et al., 2019). Regardless of how salt was deposited, our conceptual model assumes that Red Sea brine pools, replete with extremophile microbes, episodically occupied the evaporitic basin during its 7.8 mya desiccation phase (Figure 1b). Assuming those microbes had similar metabolisms to their modern descendants, we contend that the Mid Miocene evaporites should be abundantly interbedded with metalliferous sediments.

By the Late Miocene (5 mya), a connection between the Red Sea and the Indian Ocean was established, reflooding the basin (Mitchell et al., 2021; Pensa, Baby, et al., 2025). At that time, we assume that the surface of the Ghawwas Formation was directly exposed to the inflowing seawater, again producing large quantities of brine, which are capable of hosting assemblages of metal-enriching microbial communities (Figure 1c). As the deposition of hemipelagic mud into the basin would have swiftly sealed the exposed evaporites from the overlying seawater, we envision this enrichment episode to have been brief but spatially extensive, because of the pervasive extent of Miocene evaporites, which likely exceeded 150,000 km^2 in area five million years ago. Our model suggests that the resulting metal-enriched sedimentary horizon was later buried under the 200–300 m overburden of Quaternary sediment which now caps the Miocene stratigraphy (Baby et al., 2024; Mitchell et al., 2015; Pensa, 2024; Rowlands et al., 2014).

Today, albeit small and rare, brine pools remain a consistent feature of the modern Red Sea (Figure 1d) and form in one of two settings. First, brine pools occupy many of the “deeps” along the rift's spreading axis (Backer & Schoell, 1972; Laurila et al., 2015; Swallow & Crease, 1965; Zierenberg, 1990), though it should be noted that not all deeps boasting metalliferous sediments contained brine, as theorized by Pierret et al. (2010). The second setting for modern Red Sea brine pools occurs along the rift shoulders, where fault blocks enable modern seawater to percolate into the subsurface, dissolve underlying Miocene evaporites, and subsequently return to the seabed as brine. This brine accumulates in topographic depressions, forming brine pools. The NEOM brine pools which we recently discovered in the Gulf of Aqaba (Duchâtellier et al., 2024; Minch et al., 2024; Purkis et al., 2022, 2025) are one such example, as are the Thuwal Seeps (Batang et al., 2012) and the Afifi Pool (Duarte et al., 2020), located in the central and southern Red Sea, respectively.

Framed by our understanding of the geological history of the Red Sea, we reexamine the NEOM brine pools, located in the Aragonese Deep, and quantify the microbial enrichment of metals and trace elements to understand the ability of microbes to concentrate potentially vast metalliferous deposits earlier in the basin's history. Next, we examine a newly discovered extinct brine pool in the Hume Deep, located in the northern Red Sea, which retains evidence of microbial metalliferous enrichment, despite the brine having drained away. While we note that these brine pools have formed in tectonically distinct provinces—the Gulf of Aqaba is a pull-apart basin versus the Red Sea rift—we believe this comparison is valuable. The processes we describe can more broadly be associated with the salinity crises and subsequent reflooding of other major rift basins, such as the Michigan Basin in the Silurian

2576604x, 2026, 6, Downloaded from https://agupubs.onlinelibrary.wiley.com/doi/10.1029/2026AV002570 by Readcube (Labtiva Inc.), Wiley Online Library on [14/10/2026]. See the Terms and Conditions (https://onlinelibrary.wiley.com/terms-and-conditions) on Wiley Online Library for rules of use; OA articles are governed by the applicable Creative Commons License

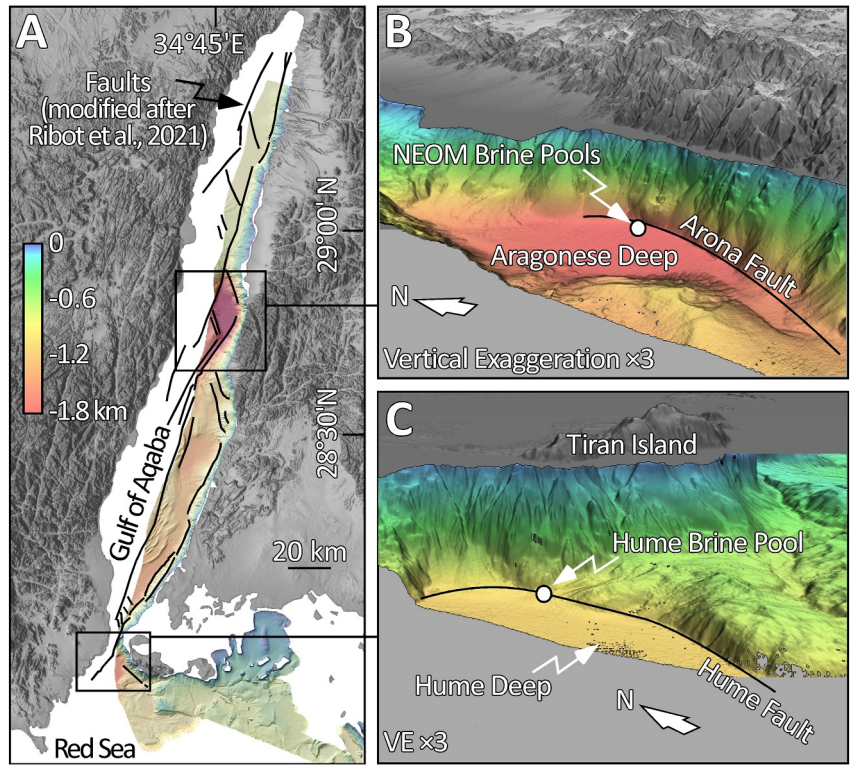


Figure 2. Location of the active NEOM and the extinct Hume Deep pools. (a) OceanX multibeam bathymetry and location of major faults in the Gulf of Aqaba. (b and c) 3-D bathymetric reconstructions showing the topography surrounding the NEOM and Hume pools.

(Cohee, 1965), the North Sea in the Permian (Brunstrom & Walmsley, 1969), the South Atlantic in the Jurassic (Nürnberg & Müller, 1991), as well as the Miocene salinity crises in the Mediterranean (Rouchy & Caruso, 2006), Persian/Arabian Gulf (Teller et al., 2000), and Caspian Basin (Van Baak et al., 2019). Our results also hold importance for the deep-time geological record. Mechanistic understanding of the formation of chemical biosignatures in well-constrained modern extreme environments provides an important process-based understanding that is critical to the accurate reconstruction of conditions that fostered the rise of early life on Earth (Anbar & Knoll, 2002; Fischer et al., 2016; Johnson et al., 2013; Lyons et al., 2014). Our work is timely because demand for metals required for the energy transition has renewed interest in marine mineral resources (Jones, 2023; Vysetti, 2023). Although current exploration efforts primarily target polymetallic nodules, cobalt-rich ferromanganese crusts, and seafloor massive sulfides, we contend that deep-sea metalliferous sediments will become increasingly important.

3. Materials and Methods

3.1. Sampling the NEOM and Hume Brine Pools With a Remotely Operated Vehicle

This study considers two brine pools. First, the active NEOM pool in the Gulf of Aqaba (Purkis et al., 2022), which we discovered in 2022 at a depth of 1,770 m in the Aragonese Deep pull-apart basin (Figure 2). Our second site, the Hume pool, is in the northern Red Sea rift, offshore the Midyan Peninsula off the southwest coastline of Tiran Island. The Hume pool is situated at a depth of 1,370 m, in the Hume Deep, another pull-apart basin. Like the NEOM pool, this site bears all the hallmarks of an active brine pool (Figure 3)—a seabed depression containing a rich Lagerstätte of calcareous metazoans, rimmed by a radically discolored "beach," directly akin to the brightly colored microbial zones which surround the NEOM pool (Figure 3c). The only component lacking from this site is the brine itself, which we presume to have drained away prior to discovery. Thus, we consider our second "Hume Deep" site to be an extinct pool. We will build evidence for this interpretation via comparison

2576604x, 2026, 6, Downloaded from https://agupubs.onlinelibrary.wiley.com/doi/10.1029/2026AV002570 by Readcube (Labtiva Inc.), Wiley Online Library on [14/10/2026]. See the Terms and Conditions (https://onlinelibrary.wiley.com/terms-and-conditions) on Wiley Online Library for rules of use; OA articles are governed by the applicable Creative Commons License

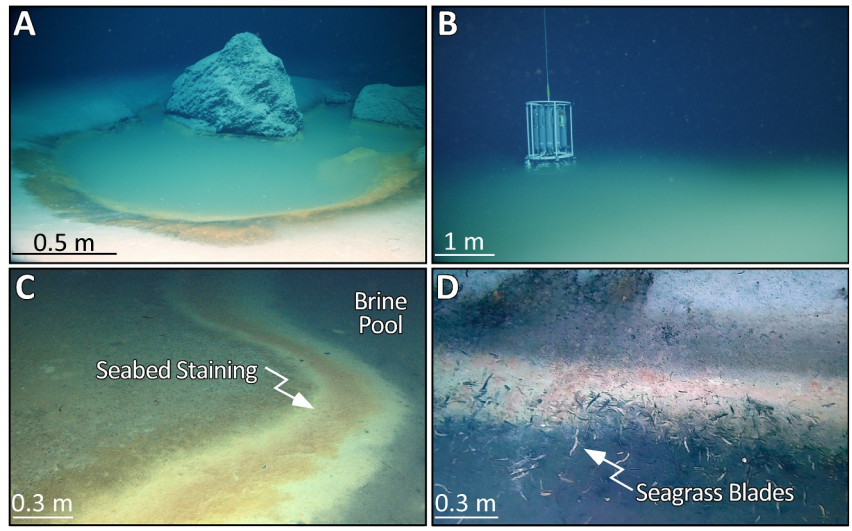


Figure 3. Remotely Operated Vehicle (ROV) photographs of the active NEOM brine pool. (a) Small brine "pond" situated 25 m west of the main (10,000 m^2) pool. (b) Conductivity, temperature, and density sensor (CTD) being lowered through the brine-seawater interface. (c) Microbially stained seabed, encircling the main brine pool. (d) Seagrass blades trapped in the brine. Again, note microbial staining of the pool's rim.

between the elemental compositions of the sediment accumulating on the regular bathyal Red Sea seabed, versus those that accumulate in the active and extinct brine pools.

We sampled our five study sites; an active pool (two surface samples and three subsurface), a potentially extinct pool (five surface samples), and three regular seabed sites (five surface samples), during 2020, 2022, and 2023 research expeditions aboard the R/V OceanXplorer. Using a Mariner XL Argus remotely operated vehicle (ROV) equipped with two 7-function hydraulic manipulators and high-definition cameras, we collected surficial sediments from each location, which were placed into sealed vessels at the seabed, so as to prevent loss of fine material and contamination during the ascent of the vehicle. The ROV position was determined by integrating its acoustically tracked position relative to the dGPS-equipped mother ship with the vessel's GPS coordinates (measured to be cm-precision), providing continuous georeferenced navigation at the seabed, with <0.5 m precision. Each of the 12 surficial samples were collected from the sediment-water interface down to a depth of 10 cm beneath the seabed, and weighed at least 50 g. Sample site locations are reported in accompanying Data Set S1, https://doi.org/10.6084/m9.figshare.29113793.v1.

To supplement our surficial sediment samples from the active pool, we also extracted four additional samples from a core taken from the NEOM brine pool analyzed by Purkis et al. (2022, 2025), for which robust ^{14}C age models have already been established (Figure S1 in Supporting Information S1). This record extends from the present day back to 1.6 kyr (±0.21 kyr), enabling us to audit the elemental composition of the stratigraphy beneath the NEOM pool. Prior to subsampling, we used X-ray fluorescence (XRF) scans and sediment facies observations to guide interval selection, targeting horizons with elevated Mn and Fe counts that were most likely to capture phases of enhanced metalliferous enrichment (Figure S1 in Supporting Information S1). The four downcore intervals which we sampled explicitly avoided turbidite layers, so as to ensure the geochemical record reflected in situ depositional conditions rather than episodic disturbance.

3.2. Geochemistry, Geochronology, and Genetics

We conducted a multi-step quantitative sequential leaching protocol to quantify the concentrations of metals and trace elements associated with different compositional fractions in our sediment samples, including sedimentary organic matter, carbonate minerals, and iron-manganese oxides (Figure S2 and Table S1 in Supporting Information S1). Analyses were conducted using triple quadrupole inductively coupled plasma mass spectrometry (Agilent 8900 ICP-QQQ) as previously described by Pollier et al. (2025), measuring manganese (Mn), iron (Fe), molybdenum (Mo), copper (Cu), and potassium (K). All concentrations were normalized to mass loss for each step in the sequential leaching protocol. Accuracy of the method was assessed through analysis of multiple

2576604x, 2026, 6, Downloaded from https://agupubs.onlinelibrary.wiley.com/doi/10.1029/2026AV002570 by Readcube (Labtiva Inc.), Wiley Online Library on [14/10/2026]. See the Terms and Conditions (https://onlinelibrary.wiley.com/terms-and-conditions) on Wiley Online Library for rules of use; OA articles are governed by the applicable Creative Commons License

2576604x, 2026, 6, Downloaded from https://agupubs.onlinelibrary.wiley.com/doi/10.1029/2026AV002570 by Readcube (Labtiva Inc.), Wiley Online Library on [14/10/2026]. See the Terms and Conditions (https://onlinelibrary.wiley.com/terms-and-conditions) on Wiley Online Library for rules of use; OA articles are governed by the applicable Creative Commons License

certified reference materials and SPEX CertiPrep solutions, with average percent recovery always greater than 90% for all analytes of interest. Full methodological details and assessment of accuracy can be found in Supporting Information S1. Then, we used metagenomic and metatranscriptomic analyses to determine the composition, metabolic pathways, and activity levels of the extremophile bacterial and archaeal communities. This was achieved using total mRNA and total eDNA extraction, short-read whole genome and transcriptome sequencing, and metagenomic binning to recover bacterial metagenome assembled genomes (MAGs). Protein prediction of these MAGs was used to identify microbial metabolic pathways, and transcriptome reads were utilized to quantify the expression of these pathways relating to enriched metals. Scanning electron microscopy (SEM) was used to image the microbes, and energy-dispersive X-ray spectroscopy (EDS) to quantify the elemental enrichments on their surfaces. Lastly, to establish when the Hume Deep pool last contained brine, we determined the age of 14 echinoderm skeletons from the pool's Lagerstätte using uranium-thorium geochronology. All digestions were filtered through 0.22 μm PFA filters and spiked with a calibrated $^{229}Th/^{233}U/^{236}U$ tracer for isotope dilution mass spectrometry. Spike calibration and external normalization were conducted using certified reference materials IRMM-35 (Th) and CRM-112a (U). A detrital $^{230}Th/^{232}Th$ activity ratio of 0.6 ± 0.2 was applied to correct for excess ^{230}Th. The measured skeletons were collected along a transect across the seabed depression containing the Lagerstätte, with each sample separated by at least 25 m. Full methodological details for all these analyses is provided in our accompanying Supplemental Information.

4. Results

4.1. Depositional Setting of the Active NEOM and Extinct Hume Deep Brine Pools

The NEOM pool in the Gulf of Aqaba is active (presently brine filled) and situated at 1,770 m in the Aragonese Deep (Figure 2b). Our second site, the Hume Deep pool in the northern Red Sea, is extinct, now devoid of brine, and lies at a depth of 1,370 m offshore Tiran Island (Figure 2c). Both pools situate atop active transform faults associated with pull-apart basin mechanics. The Arona fault passes beneath the NEOM pool and the Hume fault beneath the Hume pool (Ribot et al., 2024).

The 10,000 m^2 NEOM pool is surrounded by several small brine "ponds," each only a few m^2 in area. Our coring of this area suggests that the shallow subsurface of at least the eastern side of the Aragonese Deep is saturated with brine (Purkis et al., 2022), akin to a terrestrial water table. Configured as such, any seabed depression deeper than the "brine table" fills with brine, turning seabed depressions into brine pools—for example, Figures 3a and 3b. We hypothesize that the brine filling the Aragonese Deep (and subsequently, the NEOM pools) is sourced from the interaction of seawater in the subsurface with the underlying sediments and evaporitic formations along transform faults.

A belt of dense microbial communities surrounds each of the NEOM pools. This belt, varying in width from 1 to 3 m, neatly divides into three distinct zones based on the seabed coloration induced by the resident microbial assemblages—the "gray shoreward," "orange," and "gray brineward" zones (Purkis et al., 2022) (Figure 3c).

Despite the lack of brine, the Hume Deep site displays two visual hallmarks which suggest it to be an extinct pool. First, a seabed depression is ringed by a belt of discolored sediment (Figures 4a and 4b), mimicking the microbial zones surrounding the active NEOM pools (Figure 3c). In addition, both depressions are filled with an abundant death assemblage of calcareous metazoans—a Lagerstätte—explored in the following section.

4.2. Brine Pools as Lagerstätte Traps

Many brine pools act as Lagerstätte traps (Bäcker & Richter, 1973; Purkis et al., 2022), though, in rare cases, taphonomic processes can degrade shells and skeletons over time (Parsons-Hubbard et al., 2011). When exposed to anoxic brine, metazoans (animals) swiftly asphyxiate, die, and their shells and skeletons accumulate beneath the brine. The bed of the NEOM pool is veneered by a "hash" of fish bones and scales, plus pteropods, foraminifera, gastropods, sponge spicules, brachiopods, serpulid worms, and piles of intact echinoid skeletons. The brine also effectively preserves organic matter; abundant seagrass blades float on the surface of the NEOM pool (Figure 3d), despite it being located nearly 2 km beneath the photic zone, similar to the observations of Stuhr et al. (2025).

The now-brineless depression in the Hume Deep is filled with the same death assemblage as the NEOM pool (Figure 4). Echinoid skeletons have accumulated there in a similar composition, along with the same

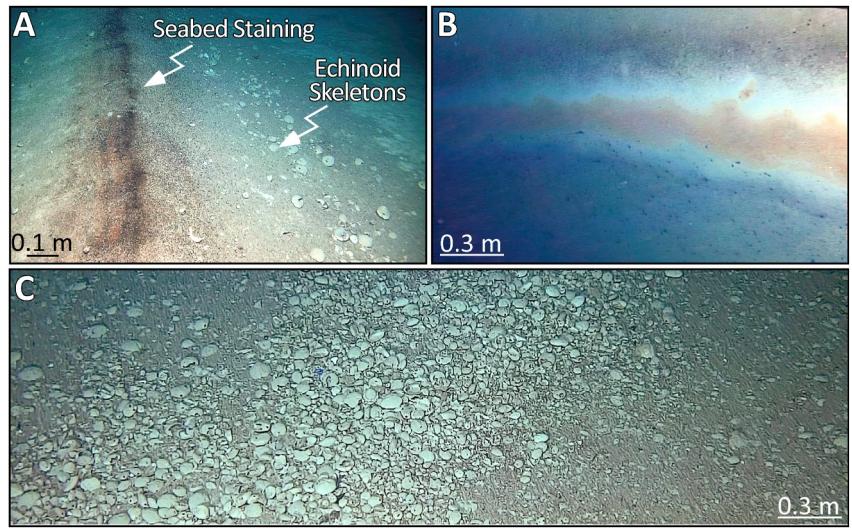


Figure 4. Remotely Operated Vehicle (ROV) photographs of the extinct Hume Deep brine pool. (a) Lagerstätte death assemblage. Note abundant echinoid skeletons and stained sediment rimming the depression, shown also in panels (b and c), respectively.

characteristic calcareous hash (Figure 5). Skeletal grains are strikingly more abundant at the Hume and NEOM sites compared to the regular bathyal seabed of the Gulf of Aqaba. In surficial samples collected by ROV, the ratio of skeletal to non-skeletal grains is approximately equal (1:1.1 for Hume and 1:1.0 for NEOM). In stark contrast, regular bathyal seabed samples are dominated by siliciclastic grains, with approximately 99 non-skeletal grains for every skeletal one (Figure 5). The two pools evidently serve as highly effective passive-entrapment Lagerstätte traps. The active NEOM brine pool and extinct Hume Deep pool are identical in this regard.

4.3. Hume Brine Pool Activity Spanned at Least 14 kyr

We presume that the abundant echinoid death assemblage present in the Hume depression (Figure 5) represents individuals that wandered into the pool during its active phase(s), asphyxiated and died in the anoxic conditions, and became incorporated in the Lagerstätte. This assumption seems reasonable, given that dead echinoids are exceedingly rare on the regular seabed which we surveyed. There, we only encountered three such skeletons in over 75 km of ROV transects recorded across the bathyal seabed of the northern Red Sea and Gulf of Aqaba. By contrast, many tens of echinoid skeletons can be found in each square meter of the brine pool Lagerstätte. To quantify this disparity in abundance, we weighed the proportion of echinoid skeletal fragments in 10-g seabed samples collected from the beds of the NEOM and Hume pools, and also from the regular seabed. The mass of echinoid skeletal fragments per 10-g sample at the NEOM site is 3.91 g ± 1.21 g over five replicates. For the Hume site, that value is 5.22 g ± 2.87 g. Meanwhile, the mass of echinoids in the regular seabed away from these two depressions, but in the same depth range, is only 0.01 g ± <0.01 g.

The ages of 14 echinoid skeletons collected from the extinct Hume brine pool ranged between 1.99 and 16.17 kyr Before Present (BP) (Figure 5d, Data Set S1, https://doi.org/10.6084/m9.figshare.29113793.v1). At the 95% confidence interval, the minimum uncertainty of these ages is ±0.25 kyr, and the maximum is ±1.52 kyr. Assuming the echinoids were killed by the anoxic conditions, these ages suggest that the Hume Deep hosted brine for at least part of the 1.99–16.17 kyr BP interval. Although these ages cannot determine whether the depression remained continuously brine-filled throughout this period, the concentration of skeletal remains within a single topographic depression may be more consistent with prolonged occupancy than with repeated episodes of drainage and refilling. The data are insufficient to distinguish conclusively between these scenarios, and open-system behavior of echinoid calcite further limits the precision of our dating, even after detrital ^{232}Th correction (see accompanying Data Set S1, https://doi.org/10.6084/m9.figshare.29113793.v1). Nonetheless, it is clear that the longevity of the active and inactive phases of this pool is measured in millennia, as opposed to centuries.

2576604x, 2026, 6, Downloaded from https://agupubs.onlinelibrary.wiley.com/doi/10.1029/2026AV002570 by Readcube (Labtiva Inc.), Wiley Online Library on [14/10/2026]. See the Terms and Conditions (https://onlinelibrary.wiley.com/terms-and-conditions) on Wiley Online Library for rules of use; OA articles are governed by the applicable Creative Commons License

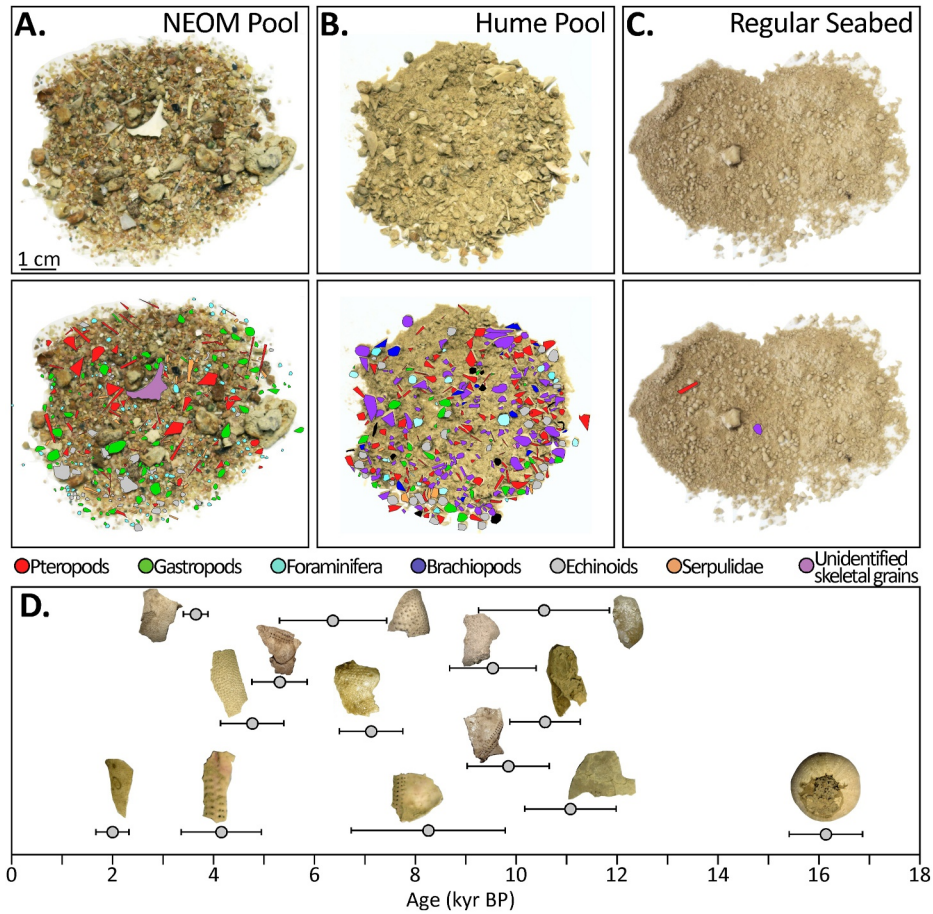


Figure 5. Representative 10-g sediment samples collected in the active NEOM brine pool (a), the extinct Hume pool (b), and the regular Gulf of Aqaba bathyal seabed (c). Sample locations shown in Figure 6. (d) Plots of uranium-thorium (U-Th) ages of 14 echinoids collected from the extinct Hume pool Lagerstätte. Error bars chart 95% confidence intervals (±0.79 kyr) around the mean ages.

4.4. Microbe-Mineral Interactions in and Around Brine Pools

A conspicuously stained band of sediment rims both the active NEOM and extinct Hume brine pools (Figures 3 and 4). For the case of the NEOM pool, extremophile brine-associated microbes occupy this zone (Minch et al., 2024; Purkis et al., 2022). Despite the absence of brine and living microbial mats in the extinct Hume pool, the seabed retains its discoloration, indicating that the residue, potentially linked to microbial activity, pigments the seabed. Sequential leaching of sediments revealed that the NEOM and Hume brine pools possess distinct chemical signatures, differentiating them from the surrounding seabed. The concentrations of five elements (Fe, K, Mn, Cu, Mo), all of which have been recognized as being associated with extremophile microbial activity (Dong et al., 2022), displayed substantial enrichments in the organic matter fraction of the sediments associated with the NEOM and Hume Deep brine pools. In the surface sediments, total iron (Fe) concentrations were enriched in brine pool-associated organic matter by a factor that ranged between 14 and 41×, potassium (K) by factors between 1–16×, manganese (Mn) by factors between 60 and 117×, copper (Cu) by 7–48×, and molybdenum (Mo) by 25–41×, when compared to organic matter associated with sediments from the regular seabed (Figure 6b, *note log y-axis,* Table S2 in Supporting Information S1).

The active microbial communities inhabiting the NEOM pool afforded a unique opportunity to investigate associations between total Fe, K, Mn, Mo, and Cu enrichments in the organic matter and microbial activity. Scanning electron microscopy (SEM) revealed abundant filamentous structures embedded within a dense matrix that is consistent with extracellular polymeric substances (EPS; Figure 7a), although we cannot exclude the possibility that some of these features represent authigenic ferromanganese precipitates. Energy dispersive

2576604x, 2026, 6, Downloaded from https://agupubs.onlinelibrary.wiley.com/doi/10.1029/2026AV002570 by Readcube (Labtiva Inc.), Wiley Online Library on [14/10/2026]. See the Terms and Conditions (https://onlinelibrary.wiley.com/terms-and-conditions) on Wiley Online Library for rules of use; OA articles are governed by the applicable Creative Commons License

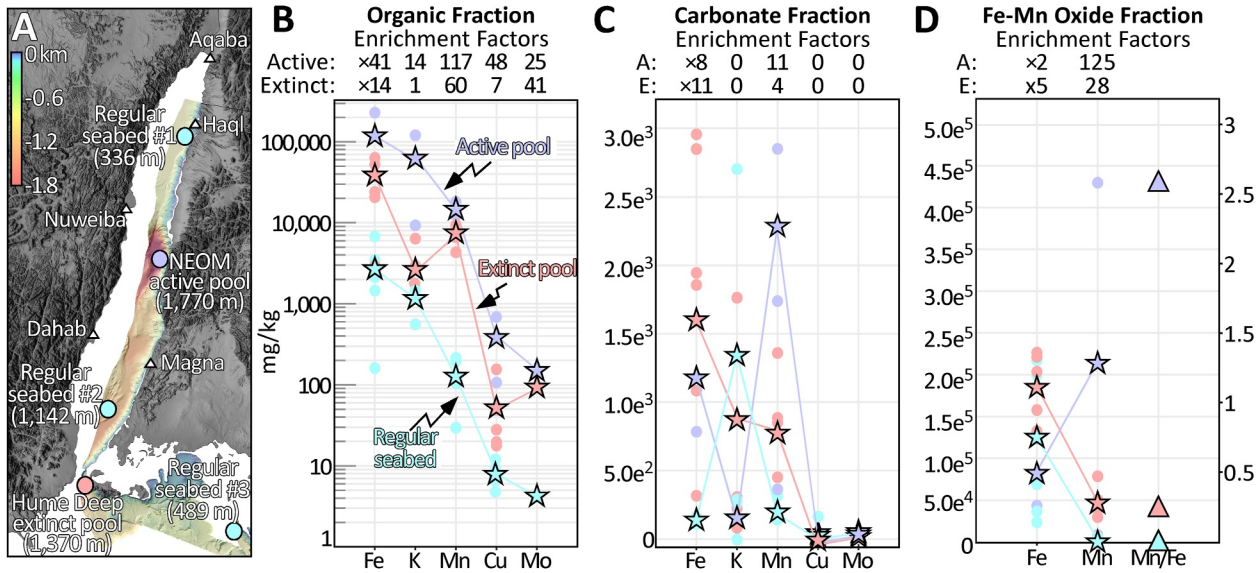


Figure 6. Elemental composition of organic matter, carbonate, and Fe-Mn oxides collected from the active and extinct brine pools, and the regular seabed. (a) Multibeam bathymetry and locations of our five sample sites, with water depths as noted. (b) Log scale concentrations (mg/kg) and enrichment factors of iron (Fe), potassium (K), manganese (Mn), copper (Cu), and molybdenum (Mo), in the organic matter associated with the sediment samples isolated using a sequential leaching protocol and ICP-QQQ analyses. Circles in these plots represent measurements and stars their averages, both color-coded by site (active pool, extinct pool, and regular seabed). Mo values reflect single measurement per site. (c) Concentrations and enrichment factors of the same elements in the carbonate phase and, (d), for Fe and Mn in the oxide phase. Triangles in this last plot denote the Mn/Fe ratios in the oxide phase—secondary *y*-axis.

electron spectroscopy (EDS) analyses confirmed that Fe, K, and Mn were highly enriched on the filamentous structures (Figure 7b), whereas Mo and Cu—though identified by sequential leaching and ICP-QQQ analyses to occur at concentrations of 0.008 wt % and 0.038 wt %, respectively (Table S2 in Supporting Information S1)—remained below EDS detection thresholds (~0.1 wt %). ICP-MS analyses supported the results of SEM-EDS analyses, and showed that concentrations of Fe, K, and Mn reached 11.3 wt %, 6.4 wt %, and 1.5 wt %, respectively, in the organic matter associated with the active NEOM pool, well within EDS detection capability (Table S2 in Supporting Information S1; Figure 6). Non-microbial substrates returned zero counts for all five elements. Our EDS analyses demonstrate that elevated concentrations of Fe, K, and Mn are spatially associated with the filamentous structures and their surrounding matrix, even within extinct brine pools. Although the precision of the EDS measurements precludes a definitive determination for Mo and Cu, our combined approach of sequential leaching and ICP-QQQ analysis confirms these elemental enrichments occur in the sedimentary organic matter, and metagenomic and metatranscriptomic data clearly advocate that these elements are likewise microbially linked.

While the elemental composition of the organic matter revealed a strong association between microbial structures and metal enrichments, the elemental composition of the carbonate and Fe-Mn oxide fraction of the seabed sediments provides insight into the extent to which these metal enrichments are preserved in the geological record. Relative to the corresponding carbonate fraction of the regular seabed sediments, in the carbonate fraction of sediments collected from both the active and extinct brine pool total Fe was enriched by a factor that ranged between 8 and 11× and Mn by a factor between 4 and 11× (Figure 6c). Likewise, the Fe-Mn oxide fraction from the brine pools exhibits Fe enrichment factors between 2 and 5× and Mn by a factor between 28 and 125× relative to the Fe-Mn oxide fraction of the regular seabed sediments (Figure 6d). When examined as Mn/Fe ratios, the Fe-Mn oxide fraction from the NEOM pool displays Mn/Fe ratios of 2.60, the Hume pool presents a Mn/Fe ratio of 0.26, and Fe-Mn oxides in the sediments from the regular seabed exhibits a ratio of 0.05 (Figure 6d). Although Mn/Fe ratios alone are not uniquely diagnostic of microbial activity, since hydrogenetic and diagenetic processes can yield overlapping values (Dymond et al., 1984; Hein & Koschinsky, 2014; Usui et al., 2020), SEM-EDS results suggest that microbial filaments are associated with enrichments in Mn and Fe (Figure 7), an observation supported by genomic evidence for Fe- and Mn-oxidizing metabolisms in the microbial communities associated with these sediments (discussed in the next section).

2576604x, 2026, 6, Downloaded from https://agupubs.onlinelibrary.wiley.com/doi/10.1029/2026AV002570 by Readcube (Labtiva Inc.), Wiley Online Library on [14/10/2026]. See the Terms and Conditions (https://onlinelibrary.wiley.com/terms-and-conditions) on Wiley Online Library for rules of use; OA articles are governed by the applicable Creative Commons License

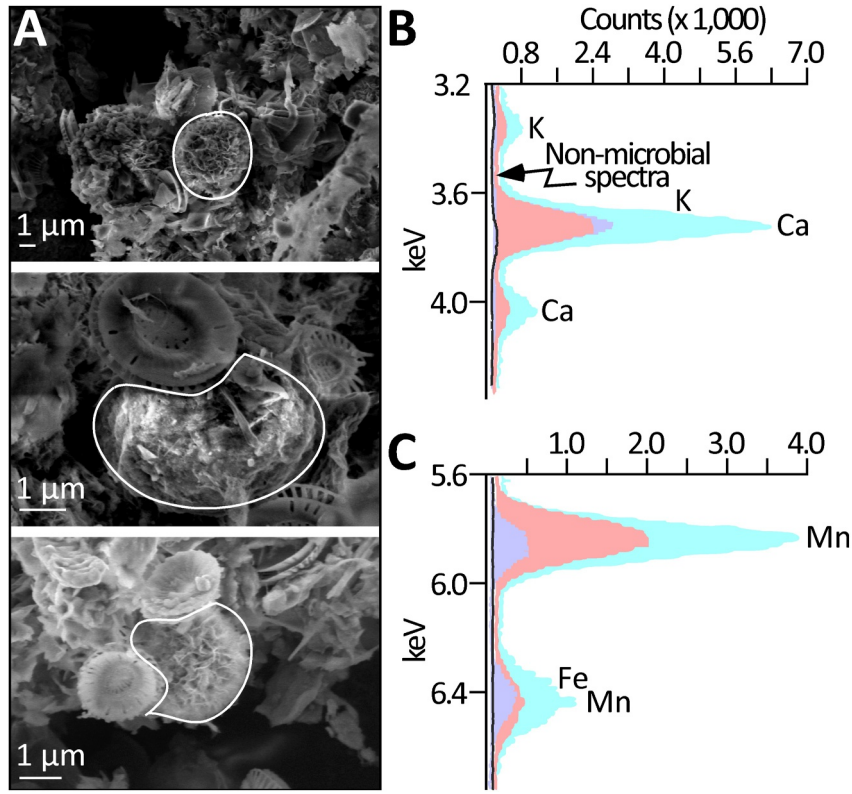


Figure 7. Scanning electron microscopy (SEM) and energy dispersive spectroscopy (EDS) of NEOM brine pool sediments and filamentous structures. (a) Representative electron micrographs (microbes circled in white). (b) EDS spectra of microbes (cyan, pink, and purple) compared to the non-microbial areas (matrix) in the targeted micrographs (black line). Note EDS peaks signaling the presence of iron (Fe), potassium (K), manganese (Mn), and calcium (Ca) on the surfaces of the scanned microbes.

Stratigraphic trends in the elemental concentrations associated with the same compositional fractions of sediment core collected from the microbial rim at the NEOM pool were also analyzed. Consistent with our surficial samples from the two brine pools, four equally spaced subsamples spanning the top to the base of the 0.75 m core (~672 yr record) recovered from the NEOM pool (Figure 8) returned higher elemental concentrations than those measured in the regular seabed. The sedimentary organic matter returned Fe enrichments ranging from 1 to 6× the regular seabed, Mn by factors between 2 and 9×, and Cu by 1–3× (Figure 8, Table S3 in Supporting Information S1). Both the carbonate and Fe-Mn oxide fraction showed higher enrichments for Mn, Fe, and Cu. In the carbonate fraction, Fe enrichments ranged from 0 to 227× compared to the regular seabed, Mn by factors between 6 and 13×, and Cu by 0–3×. Within the Fe-Mn oxide fraction, Fe enrichments ranged from 1 to 227× relative to the regular seabed, Mn by factors between 6 and 13×, and Cu by 0–3× (Figure 8, Table S3 in Supporting Information S1). Using a minimum enrichment factor of 4× for Mn, 2× as the threshold for Fe, and 2× for Cu - based on enrichments observed in the extinct and active pool (Figure 6) - similar enrichments for Mn are identified in 75% of all samples, for Fe in 42%, and for Cu in 33% (Table S3 in Supporting Information S1).

4.5. Microbial Functional Gene Analysis Reveals Metabolic Pathways

Metagenomics of the microbial communities surrounding the active NEOM pool revealed a diverse assemblage of bacterial and archaeal taxa within the three microbial mat zones—"gray shoreward," "orange," and "gray brineward," as designated by Purkis et al. (2022) (see Figure 9 and Table 1). Relative abundances were estimated by mapping metagenomic reads to metagenome-assembled genomes (MAGs) and normalizing read counts by library size and genome length using reads per kilobase per million mapped reads (RPKM). We find the gray shoreward zone, which is furthest from the brine, had the highest abundance of microbes, but the lowest microbial diversity. The orange zone, by contrast, had an intermediate microbial abundance, as compared to the two zones

2576604x, 2026, 6, Downloaded from https://agupubs.onlinelibrary.wiley.com/doi/10.1029/2026AV002570 by Readcube (Labtiva Inc.), Wiley Online Library on [14/10/2026]. See the Terms and Conditions (https://onlinelibrary.wiley.com/terms-and-conditions) on Wiley Online Library for rules of use; OA articles are governed by the applicable Creative Commons License

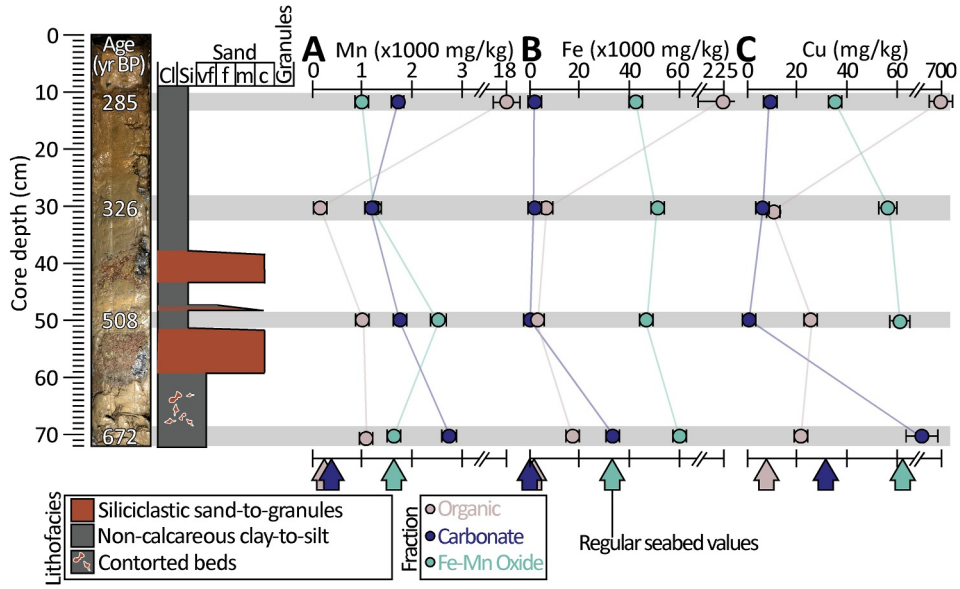


Figure 8. Downcore elemental concentrations of NEOM brine pool core sediments separated into their organic, carbonate, and Fe-Mn oxide fractions. Sample ages determined with reference to the ^{14}C model presented by Purkis et al. (2025). One sigma for these ages was determined to be ±39 years. Downcore trends in elemental concentrations: (a) Manganese (Mn), (b) Iron (Fe), and (c) Copper (Cu), for the organic matter, carbonate and Fe-Mn oxide fractions. Error bars show absolute uncertainty based on replicate measurements of certified reference materials (Table S3 in Supporting Information S1).

which flank it, yet boasted the highest diversity. Finally, the gray brineward zone, closest to the pool, had the lowest abundance of microbes and an intermediate diversity.

Across the three microbial zones, our genomic analyses revealed the presence of at least 14 bacterial and 13 archaeal families (Figure 9, Figure S3 in Supporting Information S1, and Table 1). *Gammaproteobacteria*, *Candidatus Brocadiae*, and *Gemmatimonadetes* were present in all three zones. As captured by Figure 9, other families, such as *Acidimicrobiia* and *Dehalococcpidia,* reside solely in the orange zone.

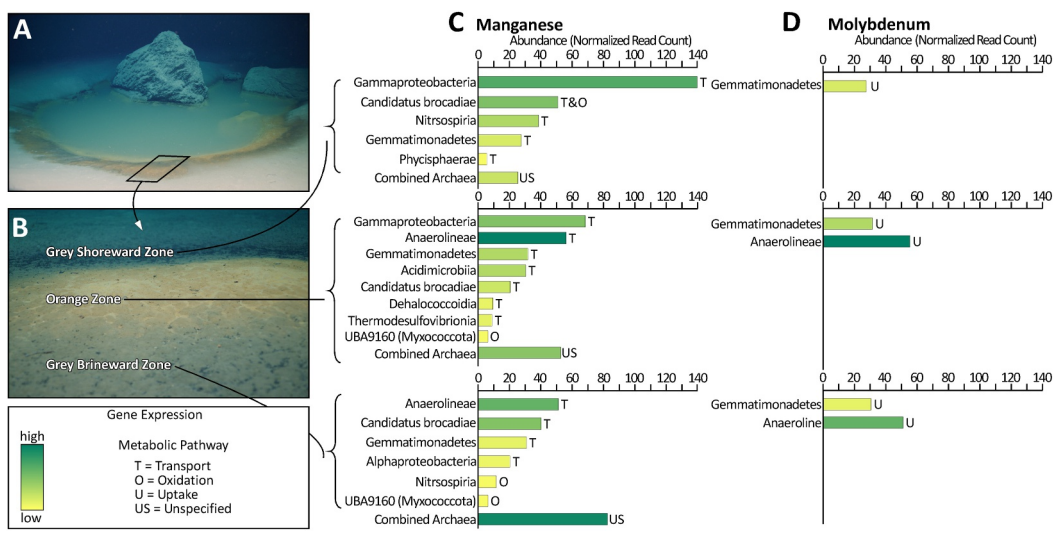


Figure 9. Active bacterial and archaeal populations encode key metabolic pathways for Mn and Mo transport, oxidation, and uptake. (a) The NEOM brine pool with the microbial mats surrounding it. (b) Close-up photograph of the three distinct microbial zones—gray shoreward, orange, and gray brineward. Microbial families which exhibit metabolic pathways that transport, oxidize, or take up manganese (c) and molybdenum (d), associated with each zone. Equivalent charts for potassium, copper, and iron as Figure S3 in Supporting Information S1.

2576604x, 2026, 6, Downloaded from https://agupubs.onlinelibrary.wiley.com/doi/10.1029/2026AV002570 by Readcube (Labtiva Inc.), Wiley Online Library on [14/10/2026]. See the Terms and Conditions (https://onlinelibrary.wiley.com/terms-and-conditions) on Wiley Online Library for rules of use; OA articles are governed by the applicable Creative Commons License

2576604x, 2026, 6, Downloaded from https://agupubs.onlinelibrary.wiley.com/doi/10.1029/2026AV002570 by Readcube (Labtiva Inc.), Wiley Online Library on [14/10/2026]. See the Terms and Conditions (https://onlinelibrary.wiley.com/terms-and-conditions) on Wiley Online Library for rules of use; OA articles are governed by the applicable Creative Commons License

Table 1
Active Microbial Families in the NEOM Brine Pool Sediments and Their Associated Metabolisms

Element	Bacterial and archaeal families	Metabolic pathway
Manganese (Mn)	*Gammaproteobacteria*	Transport
	Candidatus Brocaidae	Transport/Oxidation
	Nitrospriria	Transport
	Gemmatimonadetes	Transport
	Phycisphaerae	Transport
	Anaerolineae	Transport
	Acidimicrobiia	Transport
	Dehalococcoidia	Transport
	Thermodesulfovibrionia	Transport
	Myxococcota	Oxidation
	Alphaproteobacteria	Transport
	Archaea	Unspecified metabolism
Copper (Cu)	*Gammaproteobacteria*	Resistance/Regulation
	Candidatus Brocaidae	Resistance/Regulation
	Anaerolineae	Resistance/Regulation
	Thermodesulfovibrionia	Resistance/Regulation
	Myxococcota	Resistance/Regulation
	BMS3Abin14	Resistance/Regulation
	Microgenomatia	Resistance/Regulation
	Archaea	Resistance
Potassium (K)	*Gammaproteobacteria*	Solubility
	Candidatus Brocaidae	Solubility
Molybdenum (Mo)	*Gemmatimonadetes*	Uptake
	Anaerolineae	Uptake
Iron (Fe)	*Gammaproteobacteria*	Acquisition/Reduction/Storage
	Gemmatimonadetes	Acquisition
	Nitrospirales	Acquisition
	Candidatus brocialles	Oxidation
	Desulfobacteria	Storage

Using metagenomic binning, we were able to recover 127 representative bacterial and archaeal metagenome-assembled genomes (MAGs) from all three zones. From this genomic information, we identified multiple metabolic pathways within the microbial genomes which could be related to metabolisms involving K, Mn, Cu, Mo, and Fe. Pairing these data with metatranscriptomics, we identified that five bacterial families were able to oxidize and transport Mn, with *Gammaproteobacteria* having the highest expression of these pathways in the gray shoreward communities and *Anaerolineae* having the highest expression within the orange and gray brineward zones (Figure 9c). In addition, two bacterial families expressed Mo uptake pathways (*Gemmatimonadetes* and *Anaerolinea*) (Figure 9d). Many of these bacterial families also had pathways relating to K solubility, Cu regulation, and Fe acquisition, reduction, storage and oxidation. This indicates the importance of K^+ homeostasis under hypersaline stress (Stautz et al., 2021) in this environment (Figures S3c–S3e in Supporting Information S1), as well as detoxification strategies employed by bacterial communities for dealing with Cu and other metal detoxification (Hanna, 2015), and mechanisms for sustaining Fe homeostasis and redox balance in metal-rich, anoxic environments (Straub et al., 2001).

In contrast to the abundant bacteria, the 13 archaeal families were comparatively rare in the NEOM pool (*Candidatus Altiarchaeales, Candidatus Bathyarchaeota, Candidatus Cenarchaeum, Nitrososphaeria, Archaeoglobi, candidate division MSBL1, Candidatus Heimdallarchaeota, Candidatus Methanophagaceae, Candidatus*

2576604x, 2026, 6, Downloaded from https://agupubs.onlinelibrary.wiley.com/doi/10.1029/2026AV002570 by Readcube (Labtiva Inc.), Wiley Online Library on [14/10/2026]. See the Terms and Conditions (https://onlinelibrary.wiley.com/terms-and-conditions) on Wiley Online Library for rules of use; OA articles are governed by the applicable Creative Commons License

Micrarchaeota, Candidatus Pacearchaeota, Candidatus Thorarchaeota, Candidatus Woesearchaeota, Thermoplasmatales). Archaea were most abundant and most active in the pool's gray brineward zone and decreased with distance from the brine (Figure 9). Given the low abundance of archaea in our samples, we lumped the 13 families to assess their combined metabolic function as it pertains to elemental enrichment. Similar to the bacterial families, metatranscriptomics reveals that the archaea also express metabolisms involving manganese (unspecified) and copper (resistance) (Figure 9c). In aggregate, our results reveal a clear relationship between metal enrichment and the activity of specific microbial communities surrounding the brine pool (Figure 9, Figure S3 in Supporting Information S1, and Table 1).

5. Discussion

5.1. Red Sea Rift-Shoulder Brine Pools Are Ephemeral

Our discovery of an extinct pool in the Hume Deep shows that Red Sea brine pools can be ephemeral on the scale of thousands of years—for this pool, we have built a case that the active brine-filled phase was only transient. While the origin of metalliferous sediments remains debated in other locations, the multidisciplinary lines of evidence derived from sediments and microorganisms collected from the Hume Deep are far more compelling. For example, in the Thetis Deep, Scholten et al. (1991) suggested that this depression, which situates on the Red Sea's central spreading axis, may have been intermittently filled with brine, which is the reason for the areas' metal rich sediments. Pierret et al. (2010) challenged that interpretation, though, proposing a purely hydrothermal source for the metalliferous sediments. It would seem that the jury is still out as to whether the Thetis Deep hosted an ephemeral pool. By contrast, the case for an extinct pool in the Hume Deep is well supported. First, save for brine, it displays all the characteristics of an active pool—an abundant Lagerstätte death assemblage, seabed staining consistent with past microbial habitation, plus sediments and organic matter with the same elemental enrichment patterns as the brine-filled NEOM pool (Figures 3–6). Any one of those observations might not conclusively indicate that the Hume Deep contains an extinct pool, but the consistent support of all three proxies provides convincing evidence for this conclusion.

U-Th dating of 14 echinoid skeletons collected from the Hume Deep's Lagerstätte assemblage span dates ranging from 1.99 to 16.17 kyr BP. Whereas we presume that the dated echinoids in the Lagerstätte were asphyxiated in brine, the precision of the dating (±0.79 kyr) and limited number of samples mean that we cannot infer whether the pool was continuously active across that time period. However, it would seem reasonable to suppose that the brine in the Hume pool drained away several centuries to millennia ago. What might have caused the brine to soak away?

Observational and geochemical data sets, including temperature, salinity, dissolved oxygen, and ionic concentrations, of the brine and sedimentary porewaters associated with the active NEOM pool made by Purkis et al. (2022) and Duchâtellier et al. (2024) suggest it to have been sourced from dissolution of subsurface Miocene evaporites, with only a very limited influence from hydrothermal activity. Note too that both the active NEOM and extinct Hume Deep pools situate atop active transform faults (the Arona and Hume faults, respectively—Figure 2). We imagine that a slip of the Hume fault might have disrupted the subsurface seawater flow responsible for filling that pool with brine. Once isolated from the source of dissolving subsurface evaporites, the brine in the depression would dissipate. Certainly, the Hume fault is active—it splays off of the Dead Sea strike-slip fault (Ribot et al., 2021, 2024), which ruptures with a recurrence frequency of once every ∼560 years (Bektaş et al., 2024). A seismotectonic "turn on/turn off" lifecycle of fault-associated brine pools on the Red Sea rift shoulders seems plausible.

An alternative mechanism for brine dispersal over time is diffusion into the overlying seawater. However, the brine–seawater interface of the active NEOM pool is exceptionally sharp (Figure 3), and measurements of salinity, oxygen, and temperature by Purkis et al. (2022) indicate that any diffusive boundary layer above the pool is extremely thin (<2 cm). If diffusion across the brine pool-seawater interface is occurring at all, it did not appear to be driving meaningful brine loss at the time of our fieldwork. Although strong currents could enhance diffusive loss, our observations and models (Purkis et al., 2025), consistent with the simulations of Yao et al. (2014), indicate that bottom currents at both sites are exceedingly weak (<0.05 m s^{-1}). Given the similarities in the hydrodynamic and tectonic settings, we consider it unlikely that the Hume pool was emptied by diffusion alone and posit that the seismotectonic activity along transform faults interacting with the subsurface Miocene evaporites provides a more likely mechanism that explains the "turn on/turn off" of Red Sea rift-shoulder brine pools.

5.2. Metal Enrichment in Salt Giant Basins

Sediments from the Hume Deep pool suggest that metals and trace elements remain enriched by factors of 10× to 117× higher than the regular seabed in their organic matter, carbonate and Fe-Mn oxide fractions, even millennia after the brine drains away (Figures 3c and 4b). Evidently, microbes are highly efficient at concentrating metals and trace elements from brine into the organic matter and sediments beneath and surrounding active brine pools, consistent with the findings of previous studies (Pollier et al., 2025). Forty-six percent of sediments subsampled from our short core in the NEOM pool show enrichment factors consistent with those observed in the active and extinct brine pools, demonstrating persistence over hundreds of years in the sedimentary record preserved beneath the pool (Figure 8).

While modern Red Sea brine pools are rare and occupy only a negligible portion of the basin, the known geological, tectonic, and sedimentary history described in our conceptual model (Figure 1) suggests that during and immediately following the Miocene salinity crisis, such pools were likely to have been large and widespread.

In the Red Sea, metalliferous sediments have only been interpreted to be deposited due to (abiotic) hydrothermal activity (Anschutz et al., 1995; Modenesi & Santamarina, 2022; Zierenberg & Shanks, 1988). Our model suggests two biological windows to open for largescale deposition of metals and trace elements by brine-pool associated microbes. First, during the salinity crisis, we anticipate brine pools were common in the partially desiccated basin (Figure 1b). Given that the deposition of the Ghawwas and Mansiyah Formations spans 14-6 myr (Pensa, Huertas, & Afifi, 2025), and given that the Red Sea was regularly recharged with seawater during its salinity crisis (Orszag-Sperber et al., 1998; Pensa, 2024; Smith & Santamarina, 2022), we propose the existence of many large brine pools at that time, all likely to be replete with critical-metal-enriching microbes.

The second biological window for metal enrichment occurs immediately after the salinity crisis, when the basin refloods for the final time (Figure 1c). Then, the top of the Ghawwas Formation is directly exposed to seawater, presumably delivering conditions that facilitate the formation of many large brine pools in the basin when the evaporites dissolve on contact with seawater. This second enrichment episode is likely to have been short lived, though, since the Ghawwas would be swiftly sealed by the accumulating overburden of hemipelagic sediment and turbidites. So sealed, brine pools would then only form along the central spreading axis of the rift, else, per our two discoveries, on the rift shoulders, associated with seismotectonic activity providing a connection to dissolving subsurface evaporites along transform faults. In this modern situation, the brine pools are inconsequential compared to their prevalence and size during and immediately after the salinity crisis.

In a stratigraphic sense, our conceptual model therefore assumes multiple laterally-continuous horizons of metalliferous sediments interleaved through the Ghawwas and Mansiyah Formations, capped by a final such layer representing the terminal reflooding of the basin. Given the fact that brine pools are evidently ephemeral on timescales of millennia, these metalliferous horizons might be anticipated to be thin. Once in the post-salt Quaternary overburden, metalliferous horizons form locally, but are volumetrically modest. As a testable model for future work, we propose that microbial activity in salt giant basins is an underappreciated driver of such stratigraphic enrichment in metals and trace elements, as recognized, for instance, in the Messinian evaporites outcropping in southeastern Spain (Boyle et al., 1985; Lu et al., 2002).

5.3. Metalliferous Brine Pool Sediments as Bioindicators of Early Life

The detection of oxidized manganese phases and molybdenum enrichments in the organic matter in the sediments collected from the NEOM and Hume brine pools provides insights into the microbial metal cycling in anoxic marine environments, a process with substantial evolutionary significance in deep time.

The presence of taxa with known Mn-oxidizing capabilities in our metagenomic data set, including *Candidatus Brocadiae, Myxococcota*, and *Nitrospira*, is consistent with the potential for microbial mediation of Mn^{2+} oxidation, likely through anaerobic or microaerophilic pathways. This co-occurrence of Mn enrichment and taxa with known Mn-oxidizing capabilities in the NEOM brine pool lends support to the hypothesis that microbial oxidation of Mn(II) to Mn oxide minerals may have occurred before the evolution of oxygenic photosynthesis, potentially acting as an early mechanism for energy production in Earth's pre-Great Oxidation Event (~2.4 Ga) biosphere (Fischer et al., 2016; Johnson et al., 2013). The microbial metabolisms and interactions with the sediments within the anoxic NEOM brine pool offer a glimpse into the biogeochemical processes that may have shaped Earth's early oceans.

2576604x, 2026, 6, Downloaded from https://agupubs.onlinelibrary.wiley.com/doi/10.1029/2026AV002570 by Readcube (Labtiva Inc.), Wiley Online Library on [14/10/2026]. See the Terms and Conditions (https://onlinelibrary.wiley.com/terms-and-conditions) on Wiley Online Library for rules of use; OA articles are governed by the applicable Creative Commons License

2576604x, 2026, 6, Downloaded from https://agupubs.onlinelibrary.wiley.com/doi/10.1029/2026AV002570 by Readcube (Labtiva Inc.), Wiley Online Library on [14/10/2026]. See the Terms and Conditions (https://onlinelibrary.wiley.com/terms-and-conditions) on Wiley Online Library for rules of use; OA articles are governed by the applicable Creative Commons License

Mo enrichments and depletions are widely used to reconstruct past ocean redox conditions, with abrupt increases in sedimentary Mo concentrations commonly interpreted as evidence of major oxygenation events (Hickman-Lewis et al., 2020; Phillips & Xu, 2021). In the NEOM pool, however, Mo enrichment may also reflect interactions among microbial communities, organic matter, and authigenic minerals. Certain microbial taxa, including *Gemmatimonadetes* and *Anaerolineae*, possess metabolic pathways that utilize Mo-containing cofactors involved in nitrogen fixation and sulfur cycling (Figures 9d and Table 1) (Anbar & Knoll, 2002; Lyons et al., 2014). Although biological uptake alone is unlikely to explain the magnitude of the observed enrichments, microbial activity, organic-matter binding, and mineral interactions may all influence Mo partitioning within the sediments (Twining & Baines, 2013). Accordingly, biological processes should be considered alongside redox-driven mechanisms when interpreting Mo enrichments in anoxic environments. Although based on a smaller sample set, Mo concentrations follow the same trends as Mn, warranting further investigation to determine the mechanisms controlling Mo enrichment.

Our data show substantial elemental enrichments within the organic matter fraction that co-occur with diverse microbial communities, with the same enrichment signal also evident in the carbonate and Fe-Mn oxide fractions of the brine-pool sediments. Downcore profiles reveal elevated enrichment factors of Fe, Mn, and Cu in 67% of the carbonate fraction relative to the surrounding seabed sediments, suggesting that microbially mediated metal enrichments can become progressively incorporated into sedimentary deposits and potentially preserved in the long-term geological record (Figure 8). Fe-Mn oxide formation has traditionally been classified as either hydrogenetic or diagenetic (Dymond et al., 1984; Hein & Koschinsky, 2014; Usui et al., 2020), although these processes do not preclude microbial mediation. Indeed, numerous studies have documented Mn-cycling microorganisms associated with deep-sea Fe-Mn deposits (Blöthe et al., 2015; Halbach, 1984; Hein & Koschinsky, 2014; Knaack et al., 2023; Shulga et al., 2022; Wang et al., 2013). Consistent with these observations, the Fe-Mn oxide fractions from the NEOM and Hume brine pools exhibit elevated Mn/Fe ratios relative to the surrounding seabed sediments (Figure 6d; Table S5 in Supporting Information S1), a characteristic reported from environments hosting Mn-cycling microbial communities. Although Mn/Fe ratios alone cannot distinguish between biogenic, hydrogenetic, and diagenetic origins (Dymond et al., 1984; Halbach, 1984; Hein & Koschinsky, 2014; Knaack et al., 2023; Shulga et al., 2022; Usui et al., 2020), *Thermosulfobacteriota* and *Nitrosopumilaceae*—bacterial families identified in Fe-Mn deposits by Shulga et al. (2022)—were also recovered in our metagenomic analyses of the NEOM brine pool sediments. Taken together, the metagenomic evidence, metal enrichments, and elevated Mn/Fe ratios support the possibility that microbial processes influence Fe-Mn cycling within Red Sea brine pools. Resolving the relative contributions of microbial and abiotic processes will require future quantification of metal fluxes, turnover rates, and reservoir sizes.

Collectively, these findings suggest that microbial elemental cycling not only shapes sediment chemistry in real time but may also contribute to distinctive elemental enrichments in sedimentary organic matter and mineral deposits that have the potential to be preserved in the stratigraphic record. The co-occurrence of Mn oxides, Mo enrichment, and diverse microbial communities in these anoxic brine systems highlights the complex interplay between microbial metabolisms and sedimentary geochemistry, potentially providing an analog environment with conditions similar to those occurring in ancient biogeochemical cycles in early Earth environments. Our metagenomic and geochemical data support active microbial Mn cycling within these anoxic microbial ecosystems, providing a modern analog for metabolic strategies that shaped Earth's early biosphere. The preservation of these geochemical and mineralogical patterns across both the organic matter and mineral (carbonate and Fe-Mn oxide) fraction suggests that Fe-Mn chemistry may preserve signals of microbial influence, although establishing such signatures as robust biosignatures of ancient microbial activity will require further work (Halbach, 1984; Hein & Koschinsky, 2014; Knaack et al., 2023; Shulga et al., 2022; Wang et al., 2013).

While anoxygenic photoautotrophic microbes are known to catalyze Fe(II) oxidation and drive metal enrichment (Kappler et al., 2005), the microbial community in the NEOM brine pool may represent an even more primitive analog—one sustained not by photosynthesis, but by chemotrophic oxidation of Mn and Fe. This pathway points to metal enrichment independent of oxygenic photosynthesis or photoautotrophy, offering a glimpse into early biogeochemical cycling on Earth. Understanding how such communities operate in deep, anoxic brines not only illuminates metal-driven microbial processes in extreme environments, but also provides a framework for exploring how microbial activity may influence geochemical signatures in ancient rocks and other planetary bodies, such as the search for life on Europa (Chirayath et al., 2022; Rithanya, 2023).

2576604x, 2026, 6, Downloaded from https://agupubs.onlinelibrary.wiley.com/doi/10.1029/2026AV002570 by Readcube (Labtiva Inc.), Wiley Online Library on [14/10/2026]. See the Terms and Conditions (https://onlinelibrary.wiley.com/terms-and-conditions) on Wiley Online Library for rules of use; OA articles are governed by the applicable Creative Commons License

6. Conclusions

Discovery of the extinct Hume Deep brine pool provides direct evidence that Red Sea brine pools are transient features, shaped by fault activity and subsurface circulation. Despite the absence of brine, the Hume Deep site retains key geochemical and biological signatures of past microbial activity, including a Lagerstätte death assemblage and metal-enriched sediments and organic matter. Our findings confirm that microbes concentrate elements associated with metals and trace elements (Fe, K, Mn, Cu, and Mo) in sedimentary organic matter, carbonate, and Fe-Mn oxides. In addition, brine pool sediments present unique Mn and Fe enrichment patterns in Fe-Mn oxides that persist for millennia after brine pool depletion. The preservation of these microbially induced elemental enrichments in sediments offers a mechanistic link between modern microbially-mediated metal accumulation and the geological record. Taken together, our data suggest that similar processes were likely to have occurred in other ancient salt giant basins, thus influencing the geochemical evolution of these important depositional environments. More broadly, our study underscores the significance of anoxic hypersaline environments in shaping the deposition of sediments with substantial elemental enrichment relevant to metals and trace elements and provides new insights into microbe-mineral interactions in extreme and anoxic deep-sea ecosystems.

Conflict of Interest

The authors declare no conflicts of interest relevant to this study.

Availability Statement

Metagenomic and metatranscriptomic reads can be found in the NCBI BioProject database under accession PRJNA1073546 (https://www.ncbi.nlm.nih.gov/bioproject/PRJNA1073546). The metagenome-assembled genomes for brine pool bacteria as well as their taxonomy can be found on figshare (Chakraborty, 2025). This data table also includes QA/QC data. U–Th geochronologic data for echinoids from the extinct Red Sea brine pool are archived on figshare (Chakraborty, 2026).

Acknowledgments

This work was carried out on the R/V *OceanXplorer* during expeditions OXR20220626 and OXR20231004. We thank the OceanX and NEOM teams for their support in developing and executing this expedition. We would also like to acknowledge the captain, crew, and all technical teams onboard R/V *OceanXplorer* for providing the platform and support for collecting this data. In particular, we thank Andrew Craig, Olaf Dieckhoff, Ewan Bason, and Kate von Krusenstiern for their assistance with data acquisition and sample collection. We also owe a debt of gratitude to our Saudi Arabian partners, NEOM, and to Richard Bush, Deborah Colbourne, Jennifer Munro, and Abdulqader Khamis for their support. Gratitude is extended to Dr. David Dauer and Natalie Zaleski for their assistance with scanning electron microscopy, and to four anonymous reviewers whose comments substantially improved our study. Our work was funded by NEOM Agreement No: SRA-ENV-2023-001/AWD-008854 to the University of Miami.

References

Ams, D. A., Swanson, J. S., Szymanowski, J. E., Fein, J. B., Richmann, M., & Reed, D. T. (2013). The effect of high ionic strength on neptunium (V) adsorption to a halophilic bacterium. *Geochimica et Cosmochimica Acta*, *110*, 45–57. https://doi.org/10.1016/j.gca.2013.01.024

Anbar, A. D., & Knoll, A. H. (2002). Proterozoic ocean chemistry and evolution: A bioinorganic bridge? *Science*, *297*(5584), 1137–1142. https://doi.org/10.1126/science.1069651

Anschutz, P., Blanc, G., & Stille, P. (1995). Origin of fluids and the evolution of the Atlantis II deep hydrothermal system, Red Sea: Strontium isotope study. *Geochimica et Cosmochimica Acta*, *59*(23), 4799–4808. https://doi.org/10.1016/0016-7037(95)00350-9

Antunes, A., Ngugi, D. K., & Stingl, U. (2011). Microbiology of the Red Sea (and other) deep-sea anoxic brine lakes. *Environmental Microbiology Reports*, *3*(4), 416–433. https://doi.org/10.1111/j.1758-2229.2011.00264.x

Baby, G., Delaunay, A., Rouby, D., Ye, J., Pensa, T., & Afifi, A. M. (2024). Sediment routing systems of the eastern Red Sea rifted margin. *Earth-Science Reviews*, *249*, 104679. https://doi.org/10.1016/j.earscirev.2024.104679

Bäcker, H., & Richter, H. (1973). Die rezente hydrothermal-sedimentäre Lagerstätte Atlantis-II-Tief im Roten Meer. *Geologische Rundschau*, *62*, 697–737.

Backer, H., & Schoell, M. (1972). New deeps with brines and metalliferous sediments in the Red Sea. *Nature Physical Science*, *240*(103), 153–158. https://doi.org/10.1038/physci240153a0

Batang, Z. B., Papathanassiou, E., Al-Suwailem, A., Smith, C., Salomidi, M., Petihakis, G., et al. (2012). First discovery of a cold seep on the continental margin of the central Red Sea. *Journal of Marine Systems*, *94*, 247–253. https://doi.org/10.1016/j.jmarsys.2011.12.004

Bektaş, Z., Avşar, U., Ribot, M., Klinger, Y., & Jónsson, S. (2024). Seismo-turbidites reveal locations of major earthquakes during the past millennium in the Gulf of Aqaba, southern Dead Sea Fault. *Earth and Planetary Science Letters*, *629*, 118595. https://doi.org/10.1016/j.epsl.2024.118595

Blöthe, M., Wegorzewski, A., Müller, C., Simon, F., Kuhn, T., & Schippers, A. (2015). Manganese-cycling microbial communities inside deep-sea manganese nodules. *Environmental Science & Technology*, *49*(13), 7692–7700. https://doi.org/10.1021/es504930v

Bostrom, K., & Peterson, M. (1966). Precipitates from hydrothermal exhalations on the East Pacific Rise. *Economic Geology*, *61*(7), 1258–1265. https://doi.org/10.2113/gsecongeo.61.7.1258

Boström, K., & Peterson, M. (1969). The origin of aluminum-poor ferromanganoan sediments in areas of high heat flow on the East Pacific Rise. *Marine Geology*, *7*(5), 427–447. https://doi.org/10.1016/0025-3227(69)90016-4

Bosworth, W., Taviani, M., & Rasul, N. M. (2018). Neotectonics of the Red Sea, Gulf of Suez and Gulf of Aqaba. In *Geological setting, palaeoenvironment and archaeology of the Red Sea* (pp. 11–35). Springer.

Boyle, E., Chapnick, S., Bai, X., & Spivack, A. (1985). Trace metal enrichments in the Mediterranean Sea. *Earth and Planetary Science Letters*, *74*(4), 405–419. https://doi.org/10.1016/s0012-821x(85)80011-x

Brunstrom, R., & Walmsley, P. J. (1969). Permian evaporites in North Sea basin. *AAPG Bulletin*, *53*(4), 870–883. https://doi.org/10.1306/5d25c805-16c1-11d7-8645000102c1865d

Camerlenghi, A. (1990). Anoxic basins of the eastern Mediterranean: Geological framework. *Marine Chemistry*, *31*(1–3), 1–19. https://doi.org/10.1016/s0304-4203(05)80002-7

Chakraborty, M. (2025). Bacterial MAGs from microbial zones around NEOM brine pool. (Version 1) [Dataset]. *Figshare*. https://doi.org/10.6084/m9.figshare.29113793.v1

Chakraborty, M. (2026). U–Th geochronology of echinoids from an extinct brine pool in the Red Sea. (Version 1) [Dataset]. *Figshare*. https://doi.org/10.6084/m9.figshare.33301863

Chakraborty, M. I., Sharifi, A., Benzoni, F., Tissot, F. L., Pourmand, A., Taviani, M., et al. (2025). Deep-water corals indicate the Red Sea survived the last glacial lowstand. *Proceedings of the National Academy of Sciences*, *122*(8), e2415559122. https://doi.org/10.1073/pnas.2415559122

Chirayath, V., Bagshaw, E., Craft, K., Dierssen, H., Lim, D., Malaska, M., et al. (2022). Oceans across the solar system and the search for extraoceanic life. *Oceanography*, *35*(1), 54–65.

Cohee, G. V. (1965). Geologic history of the Michigan Basin. *Journal of the Washington Academy of Sciences*, *55*(9), 211–223.

Corliss, J. B. (1971). The origin of metal-bearing submarine hydrothermal solutions. *Journal of Geophysical Research*, *76*(33), 8128–8138. https://doi.org/10.1029/jc076i033p08128

Corliss, J. B., Lyle, M., Dymond, J., & Crane, K. (1978). The chemistry of hydrothermal mounds near the Galapagos Rift. *Earth and Planetary Science Letters*, *40*(1), 12–24. https://doi.org/10.1016/0012-821x(78)90070-5

Craig, H. (1966). Isotopic composition and origin of the Red Sea and Salton Sea geothermal brines. *Science*, *154*(3756), 1544–1548. https://doi.org/10.1126/science.154.3756.1544

Cronan, D. S. (1979). Metallogenesis at oceanic spreading centres. *Journal of the Geological Society*, *136*(5), 621–626. https://doi.org/10.1144/gsjgs.136.5.0621

Danovaro, R., Dell'Anno, A., Pusceddu, A., Gambi, C., Heiner, I., & Møbjerg Kristensen, R. (2010). The first metazoa living in permanently anoxic conditions. *BMC Biology*, *8*, 1–10.

Debure, M., Lassin, A., Marty, N. C., Claret, F., Virgone, A., Calassou, S., & Gaucher, E. C. (2019). Thermodynamic evidence of giant salt deposit formation by serpentinization: An alternative mechanism to solar evaporation. *Scientific Reports*, *9*(1), 11720. https://doi.org/10.1038/s41598-019-48138-9

Delaunay, A., Baby, G., Fedorik, J., Afifi, A. M., Tapponnier, P., & Dyment, J. (2023). Structure and morphology of the Red Sea, from the mid-ocean ridge to the ocean-continent boundary. *Tectonophysics*, *849*, 229728. https://doi.org/10.1016/j.tecto.2023.229728

Dong, H., Huang, L., Zhao, L., Zeng, Q., Liu, X., Sheng, Y., et al. (2022). A critical review of mineral–microbe interaction and co-evolution: Mechanisms and applications. *National Science Review*, *9*(10), nwac128. https://doi.org/10.1093/nsr/nwac128

Duarte, C. M., Røstad, A., Michoud, G., Barozzi, A., Merlino, G., Delgado-Huertas, A., et al. (2020). Discovery of Afifi, the shallowest and southernmost brine pool reported in the Red Sea. *Scientific Reports*, *10*(1), 910. https://doi.org/10.1038/s41598-020-57416-w

Duchâtellier, G., Oehlert, A. M., Shernisky, H., Pollier, C. G., Swart, P. K., Howes, B., & Purkis, S. J. (2024). Sedimentary porewaters record regional tectonic and climate events that perturbed a deep-sea brine pool in the Gulf of Aqaba, Red Sea. *Science of the Total Environment*, *912*, 168804. https://doi.org/10.1016/j.scitotenv.2023.168804

Dupraz, C., Reid, R. P., Braissant, O., Decho, A. W., Norman, R. S., & Visscher, P. T. (2009). Processes of carbonate precipitation in modern microbial mats. *Earth-Science Reviews*, *96*(3), 141–162. https://doi.org/10.1016/j.earscirev.2008.10.005

Dymond, J., Lyle, M., Finney, B., Piper, D. Z., Murphy, K., Conard, R., & Pisias, N. (1984). Ferromanganese nodules from MANOP Sites H, S, and R—Control of mineralogical and chemical composition by multiple accretionary processes. *Geochimica et Cosmochimica Acta*, *48*(5), 931–949. https://doi.org/10.1016/0016-7037(84)90186-8

Fischer, W. W., Hemp, J., & Johnson, J. E. (2016). Evolution of oxygenic photosynthesis. *Annual Review of Earth and Planetary Sciences*, *44*(1), 647–683. https://doi.org/10.1146/annurev-earth-060313-054810

Gadd, G. M. (2010). Metals, minerals and microbes: Geomicrobiology and bioremediation. *Microbiology*, *156*(3), 609–643. https://doi.org/10.1099/mic.0.037143-0

Halbach, P. (1984). Deep-sea metallic deposits. *Ocean Management*, *9*(1–2), 35–60. https://doi.org/10.1016/0302-184x(84)90017-9

Hanna, M. M. A. (2015). *Metagenomic profiling of microbial metal interaction in Red Sea deep-anoxic brine pools* The American University in Cairo, AUC Knowledge Fountain.

Harris, N. (2017). *Hypersaline potash mine tailings and brine: Microbial communities and metal biosorption applications* University of Saskatchewan.

Heaton, R., Jackson, M., Bamahmoud, M., & Nani, A. (1995). Superposed Neogene extension, contraction, and salt canopy emplacement in the Yemeni Red Sea. In M. P. A. Jackson, D. G. Roberts, & S. Snelson (Eds.), *Salt tectonics: A global perspective* (Vol. 65, pp. 333–351). American Association of Petroleum Geologists. https://doi.org/10.1306/m65604c16

Hein, J. R., & Koschinsky, A. (2014). Deep-ocean ferromanganese crusts and nodules. In *Treatise on geochemistry* (Vol. 13, pp. 273–291). https://doi.org/10.1016/B978-0-08-095975-7.01111-6

Hickman-Lewis, K., Cavalazzi, B., Sorieul, S., Gautret, P., Foucher, F., Whitehouse, M. J., et al. (2020). Metallomics in deep time and the influence of ocean chemistry on the metabolic landscapes of Earth's earliest ecosystems. *Scientific Reports*, *10*(1), 4965. https://doi.org/10.1038/s41598-020-61774-w

Hovland, M., Rueslåtten, H., & Johnsen, H. K. (2015). Red Sea salt formations—A result of hydrothermal processes. In *The Red Sea: The formation, morphology, oceanography and environment of a young ocean basin* (pp. 187–203). Springer.

Hughes, G. W., Grainger, D. J., Abu-Bshait, A.-J., & Abdul-Rahman, M. J. (1999). Lithostratigraphy and depositional history of part of the Midyan region, northwestern Saudi Arabia. *GeoArabia*, *4*(4), 503–542. https://doi.org/10.2113/geoarabia0404503

Hughes, G. W. A. G., & Johnson, R. S. (2005). Lithostratigraphy of the Red Sea region. *GeoArabia*, *10*(3), 49–126. https://doi.org/10.2113/geoarabia100349

Johnson, J. E., Webb, S. M., Thomas, K., Ono, S., Kirschvink, J. L., & Fischer, W. W. (2013). Manganese-oxidizing photosynthesis before the rise of cyanobacteria. *Proceedings of the National Academy of Sciences*, *110*(28), 11238–11243. https://doi.org/10.1073/pnas.1305530110

Jones, P. (2023). Towards net-zero emissions in the global tourism industry. *Athens Journal of Tourism*, *10*(2), 125–136. https://doi.org/10.30958/ajt.10-2-3

Joye, S., MacDonald, I., Montoya, J., & Peccini, M. (2005). Geophysical and geochemical signatures of Gulf of Mexico seafloor brines. *Biogeosciences*, *2*(3), 295–309. https://doi.org/10.5194/bg-2-295-2005

Kappler, A., Pasquero, C., Konhauser, K. O., & Newman, D. K. (2005). Deposition of banded iron formations by anoxygenic phototrophic Fe(II)-oxidizing bacteria. *Geology*, *33*(11), 865. https://doi.org/10.1130/g21658.1

Knaack, D. R., Leybourne, M. I., Layton-Matthews, D., Hein, J. R., Stern, R. J., Wysoczanski, R., et al. (2023). The role of depositional environment and chemical composition on the triple oxygen isotope ratios of ferromanganese precipitates and their endmember components. *Chemical Geology*, *642*, 121785. https://doi.org/10.1016/j.chemgeo.2023.121785

Krumbein, W. E. (1983). *Microbial geochemistry*. Blackwell Scientific Publications.

2576604x, 2026, 6, Downloaded from https://agupubs.onlinelibrary.wiley.com/doi/10.1029/2026AV002570 by Readcube (Labtiva Inc.), Wiley Online Library on [14/10/2026]. See the Terms and Conditions (https://onlinelibrary.wiley.com/terms-and-conditions) on Wiley Online Library for rules of use; OA articles are governed by the applicable Creative Commons License

Laurila, T. E., Hannington, M. D., Leybourne, M., Petersen, S., Devey, C. W., & Garbe-Schönberg, D. (2015). New insights into the mineralogy of the Atlantis II Deep metalliferous sediments, Red Sea. *Geochemistry, Geophysics, Geosystems*, *16*(12), 4449–4478. https://doi.org/10.1002/2015GC006010

Lu, F. H., Meyers, W. J., & Hanson, G. N. (2002). Trace elements and environmental significance of Messinian gypsum deposits, the Nijar Basin, southeastern Spain. *Chemical Geology*, *192*(3–4), 149–161. https://doi.org/10.1016/s0009-2541(02)00009-8

Lyons, T. W., Reinhard, C. T., & Planavsky, N. J. (2014). The rise of oxygen in Earth's early ocean and atmosphere. *Nature*, *506*(7488), 307–315. https://doi.org/10.1038/nature13068

Meylan, M., Glasby, G., Knedler, K., Johnston, J., & Wolf, K. (2012). Metalliferous deep-sea sediments. *Handbook of strata-bound and stratiform ore deposits* (Vol. 9, pp. 77–178).

Minch, B., Chakraborty, M., Purkis, S., Rodrigue, M., & Moniruzzaman, M. (2024). Active prokaryotic and eukaryotic viral ecology across spatial scale in a deep-sea brine pool. *ISME Communications*, *4*(1), ycae084. https://doi.org/10.1093/ismeco/ycae084

Mitchell, N. C., Ligi, M., & Rohling, E. J. (2015). Red Sea isolation history suggested by Plio-Pleistocene seismic reflection sequences. *Earth and Planetary Science Letters*, *430*, 387–397. https://doi.org/10.1016/j.epsl.2015.08.037

Mitchell, N. C., Shi, W., Izzeldin, A., & Stewart, I. C. (2021). Reconstructing the level of the central Red Sea evaporites at the end of the Miocene. *Basin Research*, *33*(2), 1266–1292. https://doi.org/10.1111/bre.12513

Modenesi, M. C., & Santamarina, J. C. (2022). Hydrothermal metalliferous sediments in Red Sea deeps: Formation, characterization and properties. *Engineering Geology*, *305*, 106720. https://doi.org/10.1016/j.enggeo.2022.106720

Nürnberg, D., & Müller, R. D. (1991). The tectonic evolution of the South Atlantic from Late Jurassic to present. *Tectonophysics*, *191*(1–2), 27–53. https://doi.org/10.1016/0040-1951(91)90231-g

Orszag-Sperber, F., Harwood, G., Kendall, A., & Purser, B. (1998). A review of the evaporites of the Red Sea-Gulf of Suez rift. In *Sedimentation and Tectonics in Rift Basins Red Sea:-Gulf of Aden* (pp. 409–426).

Parsons-Hubbard, K. M., Brett, C. E., & Walker, S. E. (2011). Taphonomic field experiments and the role of the Shelf and Slope Experimental Taphonomy Initiative. *Palaeogeography, Palaeoclimatology, Palaeoecology*, *312*(3–4), 195–208. https://doi.org/10.1016/j.palaeo.2011.11.009

Pensa, T. (2024). Chronostratigraphy and depositional environments of the Neogene sedimentary section in the Red Sea basin.

Pensa, T., Baby, G., Teillet, T., Delaunay, A., Delgado-Huertas, A., & Afifi, A. M. (2025). Evolution of carbonate platforms in the northeast Red Sea during the last 23 million years. *Scientific Reports*, *15*(1), 1–15. https://doi.org/10.1038/s41598-025-92219-x

Pensa, T., Huertas, A. D., & Afifi, A. M. (2025). Desiccation of the Red Sea basin at the start of the Messinian salinity crisis was followed by major erosion and reflooding from the Indian Ocean. *Communications Earth & Environment*, *6*(1), 1–13. https://doi.org/10.1038/s43247-025-02642-1

Petrovic, A., Lüdmann, T., Afifi, A. M., Saitz, Y., Betzler, C., & Vahrenkamp, V. (2023). Fragmentation, rafting, and drowning of a carbonate platform margin in a rift-basin setting. *Geology*, *51*(3), 242–246. https://doi.org/10.1130/g50546.1

Phillips, R., & Xu, J. (2021). A critical review of molybdenum sequestration mechanisms under euxinic conditions: Implications for the precision of molybdenum paleoredox proxies. *Earth-Science Reviews*, *221*, 103799. https://doi.org/10.1016/j.earscirev.2021.103799

Pierret, M., Clauer, N., Bosch, D., & Blanc, G. (2010). Formation of Thetis Deep metal-rich sediments in the absence of brines, Red Sea. *Journal of Geochemical Exploration*, *104*(1–2), 12–26. https://doi.org/10.1016/j.gexplo.2009.10.001

Pollier, C. G., Reid, R. P., Suosaari, E. P., Vitek, B. E., Dupraz, C., & Oehlert, A. M. (2025). Arsenic enrichment patterns are defined by microbialite morphology, fabric, and accretion mechanism. *Nature Communications*, *16*(1), 10218. https://doi.org/10.1038/s41467-025-65007-4

Purkis, S. J., Shernisky, H., Swart, P. K., Sharifi, A., Oehlert, A., Marchese, F., et al. (2022). Discovery of the deep-sea NEOM Brine Pools in the Gulf of Aqaba, Red Sea. *Communications Earth & Environment*, *3*(1), 146. https://doi.org/10.1038/s43247-022-00482-x

Purkis, S. J., Ward, S. N., Howes, B. J., Longenecker, J. M., Chakraborty, M. I., Kalman, A., et al. (2025). A 1600-year record of extreme rainfall in northern Arabia. *Science Advances*, *11*(8), eadq3173. https://doi.org/10.1126/sciadv.adq3173

Ribot, M., Klinger, Y., Jónsson, S., Avsar, U., Pons-Branchu, E., Matrau, R., & Mallon, F. L. (2021). Active faults' geometry in the Gulf of Aqaba, southern Dead Sea Fault, illuminated by multibeam bathymetric data. *Tectonics*, *40*(4), e2020TC006443. https://doi.org/10.1029/2020tc006443

Ribot, M., Lefèvre, M., Klinger, Y., Pons-Branchu, E., Dapoigny, A., & Jónsson, S. (2024). Vertical deformation along a strike-slip plate boundary: The uplifted marine terraces of the Gulf of Aqaba and Tiran Island, at the southern end of the Dead Sea Fault. *Tectonics*, *43*(9), e2023TC007977. https://doi.org/10.1029/2023tc007977

Rithanya, B. (2023). Robotic exploration of Europa's subsurface with Autonomous Underwater Vehicle (AUV): A comprehensive mission concept and design. *Acceleron Aerospace Journal*, *1*(2), 35–38.

Rona, P. A. (1978). Criteria for recognition of hydrothermal mineral deposits in oceanic crust. *Economic Geology*, *73*(2), 135–160. https://doi.org/10.2113/gsecongeo.73.2.135

Rothschild, L. J., & Mancinelli, R. L. (2001). Life in extreme environments. *Nature*, *409*(6823), 1092–1101. https://doi.org/10.1038/35059215

Rouchy, J. M., & Caruso, A. (2006). The Messinian salinity crisis in the Mediterranean basin: A reassessment of the data and an integrated scenario. *Sedimentary Geology*, *188*, 35–67. https://doi.org/10.1016/j.sedgeo.2006.02.005

Rowlands, G., Purkis, S., & Bruckner, A. (2014). Diversity in the geomorphology of shallow-water carbonate depositional systems in the Saudi Arabian Red Sea. *Geomorphology*, *222*, 3–13. https://doi.org/10.1016/j.geomorph.2014.03.014

Scholten, J., Stoffers, P., Walter, P., & Plüger, W. (1991). Evidence for episodic hydrothermal activity in the Red Sea from the composition and formation of hydrothermal sediments, Thetis Deep. *Tectonophysics*, *190*(1), 109–117. https://doi.org/10.1016/0040-1951(91)90357-x

Segev, A., Avni, Y., Shahar, J., & Wald, R. (2017). Late Oligocene and Miocene different seaways to the Red Sea–Gulf of Suez rift and the Gulf of Aqaba–Dead Sea basins. *Earth-Science Reviews*, *171*, 196–219. https://doi.org/10.1016/j.earscirev.2017.05.004

Shulga, N., Abramov, S., Klyukina, A., Ryazantsev, K., & Gavrilov, S. (2022). Fast-growing Arctic Fe–Mn deposits from the Kara Sea as the refuges for cosmopolitan marine microorganisms. *Scientific Reports*, *12*(1), 21967. https://doi.org/10.1038/s41598-022-23449-6

Smith, J. E., & Santamarina, J. C. (2022). Red sea evaporites: Formation, creep and dissolution. *Earth-Science Reviews*, *232*, 104115. https://doi.org/10.1016/j.earscirev.2022.104115

Spooner, E., & Fyfe, W. (1973). Sub-sea-floor metamorphism, heat and mass transfer. *Contributions to Mineralogy and Petrology*, *42*(4), 287–304. https://doi.org/10.1007/bf00372607

Stautz, J., Hellmich, Y., Fuss, M. F., Silberberg, J. M., Devlin, J. R., Stockbridge, R. B., & Hänelt, I. (2021). Molecular mechanisms for bacterial potassium homeostasis. *Journal of Molecular Biology*, *433*(16), 166968. https://doi.org/10.1016/j.jmb.2021.166968

2576604x, 2026, 6, Downloaded from https://agupubs.onlinelibrary.wiley.com/doi/10.1029/2026AV002570 by Readcube (Labtiva Inc.), Wiley Online Library on [14/10/2026]. See the Terms and Conditions (https://onlinelibrary.wiley.com/terms-and-conditions) on Wiley Online Library for rules of use; OA articles are governed by the applicable Creative Commons License

Stockli, D. F., & Bosworth, W. (2018). Timing of extensional faulting along the magma-poor central and northern Red Sea rift margin—Transition from regional extension to necking along a hyperextended rifted margin. In *Geological setting, palaeoenvironment and archaeology of the Red Sea* (pp. 81–111). Springer.

Straub, K. L., Benz, M., & Schink, B. (2001). Iron metabolism in anoxic environments at near neutral pH. *FEMS Microbiology Ecology*, *34*(3), 181–186. https://doi.org/10.1111/j.1574-6941.2001.tb00768.x

Stuhr, M., Westphal, H., Marchese, F., Mateu-Vicens, G., Giovenzana, F., Lüdmann, T., et al. (2025). Seagrass-rafted large benthic foraminifera transported into the deep Red Sea. *Scientific Reports*, *15*(1), 5724. https://doi.org/10.1038/s41598-025-90047-7

Swallow, J. C., & Crease, J. (1965). Hot salty water at the bottom of the Red Sea. *Nature*, *205*(4967), 165–166. https://doi.org/10.1038/205165a0

Teller, J. T., Glennie, K. W., Lancaster, N., & Singhvi, A. K. (2000). Calcareous dunes of the United Arab Emirates and Noah's Flood: The postglacial reflooding of the Persian (Arabian) Gulf. *Quaternary International*, *68*, 297–308. https://doi.org/10.1016/s1040-6182(00)00052-5

Tubbs Jr., R. E., Fouda, H. G. A., Afifi, A. M., Raterman, N. S., Hughes, G. W., & Fadolalkarem, Y. K. (2014). Midyan Peninsula, northern Red Sea, Saudi Arabia: Seismic imaging and regional interpretation. *GeoArabia*, *19*(3), 165–184. https://doi.org/10.2113/geoarabia1903165

Twining, B. S., & Baines, S. B. (2013). The trace metal composition of marine phytoplankton. *Annual Review of Marine Science*, *5*(1), 191–215. https://doi.org/10.1146/annurev-marine-121211-172322

Usui, A., Hino, H., Suzushima, D., Tomioka, N., Suzuki, Y., Sunamura, M., et al. (2020). Modern precipitation of hydrogenetic ferromanganese minerals during on-site 15-year exposure tests. *Scientific Reports*, *10*(1), 3558. https://doi.org/10.1038/s41598-020-60200-5

Van Baak, C. G., Grothe, A., Richards, K., Stoica, M., Aliyeva, E., Davies, G. R., et al. (2019). Flooding of the Caspian Sea at the intensification of Northern Hemisphere glaciations. *Global and Planetary Change*, *174*, 153–163. https://doi.org/10.1016/j.gloplacha.2019.01.007

Vysetti, B. (2023). Deep-sea mineral deposits as a future source of critical metals, and environmental issues-a brief. *Minerals, Mining and Materials*, *23*, 25. https://doi.org/10.20517/mmm.2022.12

Wang, P., Kinraide, T. B., Smolders, E., Zhou, D.-M., Menzies, N. W., Thakali, S., et al. (2013). An electrostatic model predicting Cu and Ni toxicity to microbial processes in soils. *Soil Biology and Biochemistry*, *57*, 720–730. https://doi.org/10.1016/j.soilbio.2012.09.002

Weiss, R. (1977). Hydrothermal manganese in the deep sea: Scavenging residence time and Mn/^{3}He relationships. *Earth and Planetary Science Letters*, *37*(2), 257–262. https://doi.org/10.1016/0012-821x(77)90171-6

Yao, F., Hoteit, I., Pratt, L. J., Bower, A. S., Zhai, P., Köhl, A., & Gopalakrishnan, G. (2014). Seasonal overturning circulation in the Red Sea: 1. Model validation and summer circulation. *Journal of Geophysical Research: Oceans*, *119*(4), 2238–2262. https://doi.org/10.1002/2013jc009004

Zierenberg, R. A. (1990). Deposition of metalliferous sediment beneath a brine pool in the Atlantis II Deep, Red Sea. In *Gorda Ridge: A Seafloor Spreading Center in the United States' Exclusive Economic Zone* (pp. 131–142). Springer.

Zierenberg, R. A., & Shanks, W. C. (1988). Isotopic studies of epigenetic features in metalliferous sediment, Atlantis II Deep, Red Sea. *The Canadian Mineralogist*, *26*(3), 737–753.

References From the Supporting Information

Aroney, S. T., Newell, R. J., Nissen, J. N., Camargo, A. P., Tyson, G. W., & Woodcroft, B. J. (2025). CoverM: Read alignment statistics for metagenomics. *arXiv preprint arXiv:2501.11217*.

Bateman, A., Martin, M. J., Orchard, S., Magrane, M., Agivetova, R., Ahmad, S., et al. (2021). UniProt: The universal protein knowledgebase in 2021. *Nucleic Acids Research*, *49*(D1), D480–D489. https://doi.org/10.1093/nar/gkaa1100

Bellefroid, E. J., Planavsky, N. J., Miller, N. R., Brand, U., & Wang, C. (2018). Case studies on the utility of sequential carbonate leaching for radiogenic strontium isotope analysis. *Chemical Geology*, *497*, 88–99. https://doi.org/10.1016/j.chemgeo.2018.08.025

Chaumeil, P. A., Mussig, A. J., Hugenholtz, P., & Parks, D. H. (2020). GTDB-Tk: A toolkit to classify genomes with the Genome Taxonomy Database.

Eddy, S. R. (2011). Accelerated profile HMM searches. *PLoS Computational Biology*, *7*(10), e1002195. https://doi.org/10.1371/journal.pcbi.1002195

Eren, A. M., Kiefl, E., Shaiber, A., Veseli, I., Miller, S. E., Schechter, M. S., et al. (2021). Community-led, integrated, reproducible multi-omics with anvi'o. *Nature Microbiology*, *6*(1), 3–6. https://doi.org/10.1038/s41564-020-00834-3

Harouaka, K., Hoppe, E. W., & Arnquist, I. J. (2020). A novel method for measuring ultra-trace levels of U and Th in Au, Pt, Ir, and W matrices using ICP-QQQ-MS employing an O_2 reaction gas. *Journal of Analytical Atomic Spectrometry*, *35*(12), 2859–2866. https://doi.org/10.1039/d0ja00220h

Kang, D. D., Li, F., Kirton, E., Thomas, A., Egan, R., An, H., & Wang, Z. (2019). MetaBAT 2: An adaptive binning algorithm for robust and efficient genome reconstruction from metagenome assemblies. *PeerJ*, *7*, e7359. https://doi.org/10.7717/peerj.7359

Karlicki, M., Antonowicz, S., & Karnkowska, A. (2022). Tiara: Deep learning-based classification system for eukaryotic sequences. *Bioinformatics*, *38*(2), 344–350. https://doi.org/10.1093/bioinformatics/btab672

Li, D., Liu, C. M., Luo, R., Sadakane, K., & Lam, T. W. (2015). MEGAHIT: An ultra-fast single-node solution for large and complex metagenomics assembly via succinct de Bruijn graph. *Bioinformatics*, *31*(10), 1674–1676. https://doi.org/10.1093/bioinformatics/btv033

Li, H. (2018). Minimap2: Pairwise alignment for nucleotide sequences. *Bioinformatics*, *34*(18), 3094–3100. https://doi.org/10.1093/bioinformatics/bty191

Martin, M. (2011). Cutadapt removes adapter sequences from high-throughput sequencing reads. *EMBnet.Journal*, *17*(1), 10–12. https://doi.org/10.14806/ej.17.1.200

Pourmand, A., Tissot, F. L., Arienzo, M., & Sharifi, A. (2014). Introducing a comprehensive data reduction and uncertainty propagation algorithm for U-Th geochronometry with extraction chromatography and isotope dilution MC-ICP-MS. *Geostandards and Geoanalytical Research*, *38*(2), 129–148. https://doi.org/10.1111/j.1751-908x.2013.00266.x

Robinson, M. D., McCarthy, D. J., & Smyth, G. K. (2010). edgeR: A Bioconductor package for differential expression analysis of digital gene expression data. *Bioinformatics*, *26*(1), 139–140. https://doi.org/10.1093/bioinformatics/btp616

Sharifi, A., Biglari, F., Mashkour, M., Shidrang, S., & Taheri, K. (2023). A method for U-series dating of $CaCO_3$ crusts on Paleolithic lithic artifacts and bones and its application to Pleistocene archaeology of the Iranian Plateau. In *Goldschmidt 2023 Conference*. Goldschmidt.

Steinegger, M., & Söding, J. (2017). MMseqs2 enables sensitive protein sequence searching for the analysis of massive data sets. *Nature Biotechnology*, *35*(11), 1026–1028. https://doi.org/10.1038/nbt.3988

Suzek, B. E., Huang, H., McGarvey, P., Mazumder, R., & Wu, C. H. (2007). UniRef: Comprehensive and non-redundant UniProt reference clusters. *Bioinformatics*, *23*(10), 1282–1288. https://doi.org/10.1093/bioinformatics/btm098

2576604x, 2026, 6, Downloaded from https://agupubs.onlinelibrary.wiley.com/doi/10.1029/2026AV002570 by Readcube (Labtiva Inc.), Wiley Online Library on [14/10/2026]. See the Terms and Conditions (https://onlinelibrary.wiley.com/terms-and-conditions) on Wiley Online Library for rules of use; OA articles are governed by the applicable Creative Commons License

Tostevin, R., Shields, G. A., Tarbuck, G. M., He, T., Clarkson, M. O., & Wood, R. A. (2016). Effective use of cerium anomalies as a redox proxy in carbonate-dominated marine settings. *Chemical Geology*, *438*, 146–162. https://doi.org/10.1016/j.chemgeo.2016.06.027

Von Meijenfeldt, F. B., Arkhipova, K., Cambuy, D. D., Coutinho, F. H., & Dutilh, B. E. (2019). Robust taxonomic classification of uncharted microbial sequences and bins with CAT and BAT. *Genome Biology*, *20*, 1–14. https://doi.org/10.1186/s13059-019-1817-x

2576604x, 2026, 6, Downloaded from https://agupubs.onlinelibrary.wiley.com/doi/10.1029/2026AV002570 by Readcube (Labtiva Inc.), Wiley Online Library on [14/10/2026]. See the Terms and Conditions (https://onlinelibrary.wiley.com/terms-and-conditions) on Wiley Online Library for rules of use; OA articles are governed by the applicable Creative Commons License